https://doi.org/10.5194/essd-2026-755
Preprint. Discussion started: 22 October 2026
© Author(s) 2026. CC BY 4.0 License.



Open Access Earth System Science Data Discussions

# The European Geostrophic Wind Reconstruction (EGWR): a 220-year daily record of European geostrophic wind from surface pressure (1806–2026)

Stephan Paul[1]

[1]Technical University of Munich, School of Natural Sciences, Physics Department E18, 85748 Garching, Germany

**Correspondence:** Stephan Paul (stephan.paul@tum.de)

**Abstract.** Spatially consistent European wind observations suitable for continental-scale analysis cover only about four decades, limiting the study of infrequent and prolonged low-wind periods. We present the European Geostrophic Wind Reconstruction (EGWR), a daily record of large-scale geostrophic wind for fourteen European regions from 1806 to 2026. EGWR is derived from surface pressure in Twentieth Century Reanalysis version 3 (20CRv3) for 1806–2015 and from ERA5 thereafter. Sparse early observations smooth the ensemble-mean pressure field and systematically weaken the derived pressure gradient. A temperature-stratified decomposition identifies this as the dominant bias and attributes it to pressure-field smoothing rather than residual barometer calibration error. We correct the bias with a time-varying, region-specific, rank-preserving quantile mapping referenced to the well-observed part of the reconstruction and to ERA5.

The correction restores the wind-amplitude distribution without changing the temporal ordering of the daily record. Independent validation against ERA5, observed German wind-power generation, and two long-term anemometer records shows agreement at daily and multi-day event scales. The released dataset contains the corrected regional series together with uncertainty estimates, source and quality flags, and an optional low-frequency diagnostic. Region-specific recommended start years identify the earliest periods suitable for quantitative persistence statistics. The calibration also acts as an effective 15-year high-pass filter, removing network-driven observational drift. EGWR therefore resolves daily-to-interannual variability and persistence, whereas absolute multidecadal trends require the separately provided low-frequency diagnostic. EGWR provides an observation-based, two-century baseline for studies of European wind variability, persistence, and low-wind events.

## 1 Introduction

Long, homogeneous records of European wind are needed to characterise prolonged low-wind periods, which are of particular concern for renewable-energy supply. Direct wind observations suitable for continental-scale analysis extend back only about four decades, too short to constrain the frequency of rare, persistent events. Surface pressure, by contrast, has been measured across Europe since the early nineteenth century, and the large-scale geostrophic wind can be derived from its horizontal gradient, which offers a route to a much longer record.

https://doi.org/10.5194/essd-2026-755
Preprint. Discussion started: 22 October 2026
© Author(s) 2026. CC BY 4.0 License.



Open Access Earth System Science Data Discussions

This paper presents the European Geostrophic Wind Reconstruction (EGWR), a daily record of large-scale geostrophic wind for fourteen European regions covering 1806 to 2026. It is derived from surface pressure in the Twentieth Century Reanalysis version 3 (20CRv3) for 1806–2015 and from ERA5 thereafter. The principal obstacle to such a reconstruction is that the sparse early observing network causes the 20CRv3 ensemble-mean pressure field to smooth weather systems, so the derived wind is systematically too weak in the early decades. A temperature-stratified decomposition attributes this bias to ensemble-mean smoothing rather than to an instrument error (Sect. 4.2), which justifies an amplitude-only correction, a time-varying, region- and terrain-specific, rank-preserving quantile mapping.

The corrected record has a spatial scale of about 100 km and a daily resolution. Because the calibration acts as an effective 15-year high-pass filter that removes the network-driven observational drift, the released series resolves daily-to-interannual variability and persistence but not absolute multidecadal trends, for which a separate low-frequency diagnostic is provided (Sect. 9.3). The reconstruction is evaluated against ERA5, observed German wind-power generation, and two century-long anemometer records, none of which entered the correction. It is intended as an observation-based baseline for studies of European wind variability, persistence, and low-wind periods, and it represents large-scale geostrophic wind rather than hub-height or turbine-level wind or a derived power quantity. Rare-event drought statistics obtained from the record are analysed in a companion paper (Paul, submitted to *Nature Communications*).

---

### 1.1 Previous work and contribution

Geostrophic wind derived from sea-level pressure has a long history in European climate research (Alexandersson et al., 2000), and 20CR-based wind records have been applied to energy questions, including through distribution-based corrections against modern reanalyses (Bett et al., 2013, 2015). Such century-scale records now underpin renewable-energy and wind-drought assessments (Bloomfield et al., 2019), yet they remain difficult to homogenise: century-scale reanalyses disagree even on the sign of the multidecadal wind trend (Wohland et al., 2019), the evolving observing network introduces inhomogeneities into long reanalysis records (Krueger et al., 2013), and ensemble averaging can alter the statistics of weather extremes (Wang et al., 2012).

EGWR addresses these problems with a correction that is time-varying and specific to each region and its terrain, tied directly to the observational coverage of the reconstruction. The resulting record spans 1806 to 2026 for fourteen European regions and is evaluated against ERA5, wind-generation data, and long-term anemometer records that were not used in the correction; earlier long-record studies relied instead on other reanalyses or pressure-based proxies (Krueger and von Storch, 2011; Feser et al., 2015). The released product is a large-scale wind proxy.

https://doi.org/10.5194/essd-2026-755
Preprint. Discussion started: 22 October 2026
© Author(s) 2026. CC BY 4.0 License.



Open Access Earth System Science Data Discussions

## 2 Source data

### 2.1 The Twentieth Century Reanalysis (20CRv3)

The reconstruction is built on the Twentieth Century Reanalysis version 3 (20CRv3; Compo et al., 2011; Slivinski et al., 2019). It assimilates only historical surface-pressure observations into a weather model and provides gridded atmospheric fields back to 1806 (no wind or satellite observations are assimilated). It is the only centennial reanalysis with sub-daily fields extending back to 1806; the alternatives begin around 1900 (ERA-20C and CERA-20C; Poli et al., 2016; Laloyaux et al., 2018) or resolve only monthly means (EKF400 and ModE-RA; Franke et al., 2017; Valler et al., 2024). From it we take, for each day and region, the daily ensemble-mean sea-level pressure and near-surface temperature. The reconstruction covers 1806–2015 in two internally consistent streams of the same system, joined without a step at the end of 1980 (Sect. 6.1); because both come from the same process, its well-observed twentieth-century decades serve as the internal reference against which the sparse early years are calibrated. ERA5 is the modern reference and carries the series past 2015 (Sect. 2.4).

### 2.2 Historical pressure corrections

The pressure fields are already homogenised. Mercury-barometer readings are corrected for thermal expansion (of the mercury and the brass scale), to standard gravity and to sea level, with instrument- and station-continuity adjustments, in the International Surface Pressure Databank (Cram et al., 2015) that supplies the reanalysis. The wind bias we diagnose is therefore not a residual barometer error, verified in Sect. 4.2, but arises in the reanalysis processing.

### 2.3 Geostrophic wind from surface pressure

We do not use the near-surface wind provided by 20CRv3, which is less reliable in the sparse early record. Instead we compute the large-scale *geostrophic wind* from the horizontal pressure gradient,

$$v_g = \frac{|\nabla p|}{\rho f}, \qquad f = 2\Omega \sin\phi . \tag{1}$$

Here $|\nabla p|$ is the magnitude of the horizontal pressure gradient, $\rho \approx 1.2$ kg m$^{-3}$ the surface air density and $f$ the Coriolis parameter at latitude $\phi$, with $\Omega = 7.29 \times 10^{-5}$ s$^{-1}$ the Earth's rotation rate. The gradient is computed on the one-degree grid (about 100 km) and the resulting wind is averaged over each region. This represents the large-scale, pressure-driven wind, not the local near-surface or hub-height wind an anemometer or turbine would measure; conversion to wind power is outside the scope of EGWR (Sect. 11).

### 2.4 The modern reference (ERA5)

To judge and correct the old record, we use ERA5, the current-generation global reanalysis, covering 1940–present at high resolution from the full modern observing system. Over the 1940–1980 overlap, we compute the same pressure-derived wind

https://doi.org/10.5194/essd-2026-755
Preprint. Discussion started: 22 October 2026
© Author(s) 2026. CC BY 4.0 License.



Open Access Earth System Science Data Discussions

from each record and compare them directly. Because ERA5 is constrained by a far denser observing system, it provides the better-observed reference against which systematic bias in the historical reconstruction can be measured. We always compare the two records on the same one-degree grid, so the difference reflects the observing system rather than grid resolution.

### 2.5 The fourteen reference regions

The dataset covers fourteen reference regions (Figure 1), each covering an overlap-free set of integer-degree grid cells. Each region has a short code (used in the file names) and a descriptive name (used in text and figures); these, with the integer-degree grid box each occupies, are listed in Table 1. A country appears more than once where it spans two distinct wind climates, the boxes following that division rather than the political border: Germany is split into the North German Plain and Southern Germany, France into Northern France and the Rhône Corridor, Italy into the Po Basin and Southern Italy, and Iberia into Atlantic Iberia and the Spanish Mediterranean. The fill colour in Figure 1 shows the earliest year for which each region is reliable for quantitative extreme-value analysis, from 1806 in the densely observed north-west to around 1930 in the least-surveyed Balkan interior (Sect. 6.5).

**Table 1.** The fourteen released regions: short code, descriptive name, and the integer-degree grid box over which the geostrophic wind is averaged (Sect. 9, Figure 1).

| Code | Region | Latitude | Longitude |
|---|---|---|---|
| NOR | Southern Norway | 59–63° N | 5–11° E |
| DK | Denmark | 56–58° N | 7–13° E |
| DE-N | North German Plain | 52–55° N | 7–14° E |
| PL | Poland | 51–55° N | 15–23° E |
| EN | England | 51–57° N | 8° W–1° E |
| LC | Low Countries | 50–53° N | 2–6° E |
| DE-S | Southern Germany | 48–51° N | 7–13° E |
| FR-N | Northern France | 46–49° N | 3° W–6° E |
| IT-N | Po Basin | 44–47° N | 8–13° E |
| RO | Romania | 44–48° N | 22–28° E |
| FR-S | Rhône Corridor | 43–45° N | 2–7° E |
| IB-W | Atlantic Iberia | 37–43° N | 9–4° W |
| ES-E | Spanish Mediterranean | 37–42° N | 3° W–3° E |
| IT-S | Southern Italy | 37–43° N | 8–19° E |

### 2.6 Definition of a daily value

In 20CRv3, each daily field is the average of eight three-hourly analyses, the averaging being done on the pressure field; ERA5 is sampled on the same basis for all comparisons. Averaging the modern record in this way reduces the mean geostrophic wind by about 8% relative to a single-hour sample. As the wind direction turns through the day, the daily-mean gradient vector

https://doi.org/10.5194/essd-2026-755
Preprint. Discussion started: 22 October 2026
© Author(s) 2026. CC BY 4.0 License.

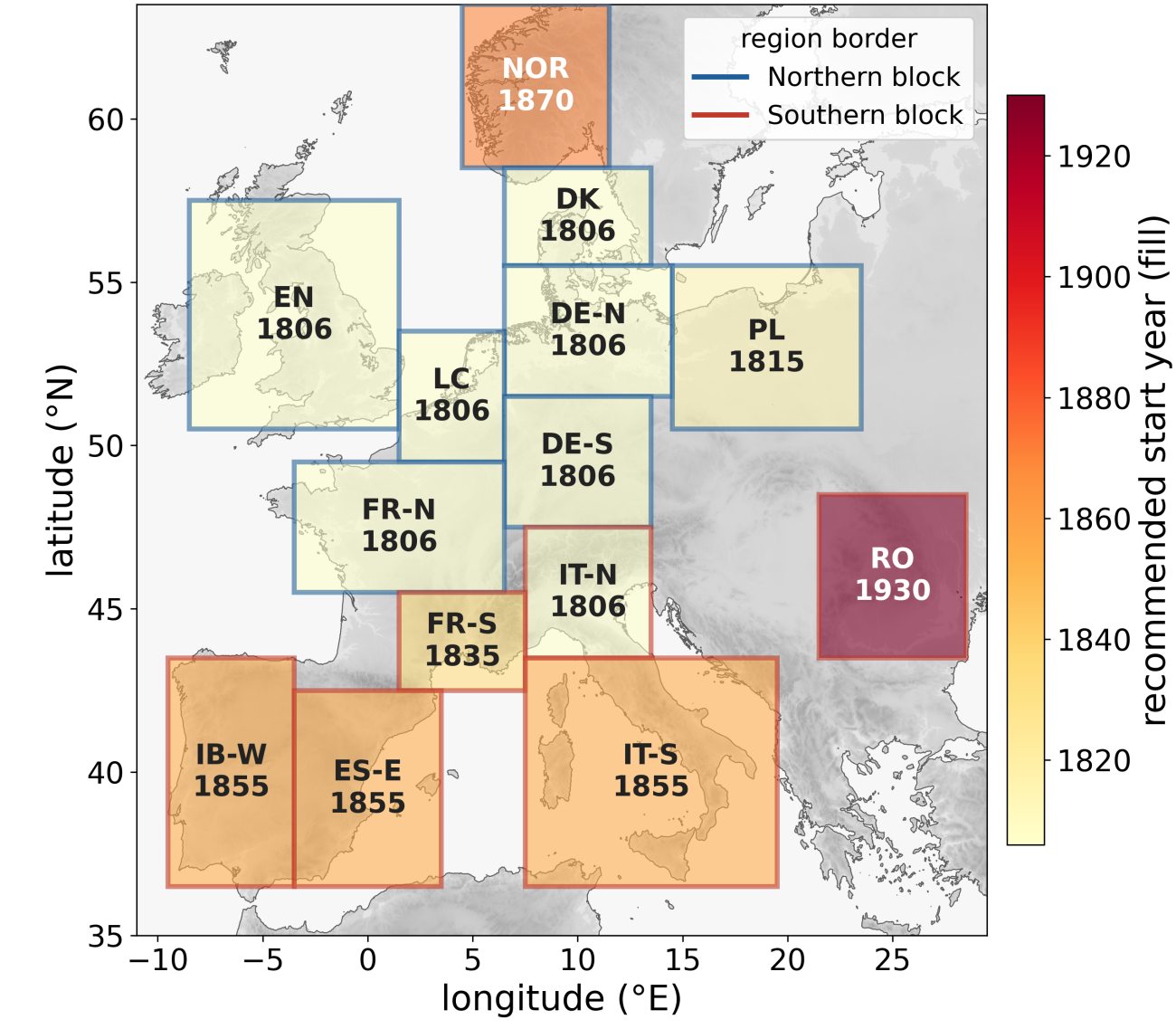



**Figure 1.** The fourteen EGWR reference regions, forming a non-overlapping tiling of the one-degree grid. Border colour indicates the northern (blue) and southern (red) synoptic blocks; fill colour shows the recommended start year for quantitative extreme-value analysis (Sect. 6.5, Table 3). Germany, France, Italy, and Iberia are each divided into separate wind-climate regions.

https://doi.org/10.5194/essd-2026-755
Preprint. Discussion started: 22 October 2026
© Author(s) 2026. CC BY 4.0 License.



Open Access Earth System Science Data Discussions

becomes smaller than the daily mean of the gradient magnitude. All comparisons of absolute wind levels therefore use the matched eight-point basis.

Daily resolution is retained because EGWR targets synoptic-scale variability and multi-day low-wind events. Sub-daily fluctuations are not resolved. In terms of wind-energy production, however, a brief gust does not interrupt a multi-day drought or the energy deficit it causes. Local thermally driven diurnal circulations (sea breezes, slope and valley flows) are likewise outside the spatial and physical scope of the product.

## 3 Stationarity of the calibration distribution

The amplitude correction assumes that the *distribution* of ordinary daily large-scale wind is approximately stable over the record. This is narrower than climate stationarity. The assumption concerns only the wind distribution used for calibration, not temperature or the rarest extremes. Observed multi-decadal wind trends are small and regionally mixed (Azorin-Molina et al., 2014; Zhang et al., 2025).

Throughout, a *wind drought* is a run of consecutive *calm* days within one extended winter (November–February, abbreviated NDJF, treated winter by winter so that no run bridges the summer gap). A day is calm when its large-scale wind falls below that region's own 20th percentile (P20) for that calendar day, taken over the whole record. Two refinements apply: an interruption of at most two days is bridged when every day in it lies below the 35th percentile (P35), since one or two marginally windy days neither break a blocking high (a stalled high-pressure system that suppresses the regional wind) nor recharge a multi-day store, and runs shorter than two days are discarded as threshold flicker. The relative threshold is unaffected by the amplitude correction (Sect. 6.3) and comparable across regions with very different mean winds.

We test this assumption over the modern ERA5 period (Figure 2). Winter wind-drought frequency shows no significant regional trend. A least-squares linear fit of the annual drought-day count against year gives a slope that is not significant in any region (all $p > 0.07$; $p$ is the probability, under the null hypothesis of no trend, of obtaining a slope at least as extreme as the observed one), the largest being $0.36\,\sigma$ per decade in Romania, even as regional temperature rises markedly (Figure 2, top). This is small compared with the interannual variability relevant to the calibration, and supports using a common reference distribution while retaining the observed temporal ordering.

## 4 Measuring the bias

### 4.1 Magnitude and time evolution of the early bias

The reconstructed wind is systematically underestimated in the early record. During 1806–1849, the pressure-derived wind is typically 20–30% below the modern reference, with the bias decreasing progressively towards 1900 (Figure 3). The change follows the historical growth of the observing network. As barometers multiplied through the nineteenth century, the reconstruction smoothed the weather less. Uncertainties are estimated with a block bootstrap; both the early shortfall and its disappearance by 1900 are statistically significant relative to these uncertainties.

https://doi.org/10.5194/essd-2026-755
Preprint. Discussion started: 22 October 2026
© Author(s) 2026. CC BY 4.0 License.



Open Access Earth System Science Data Discussions

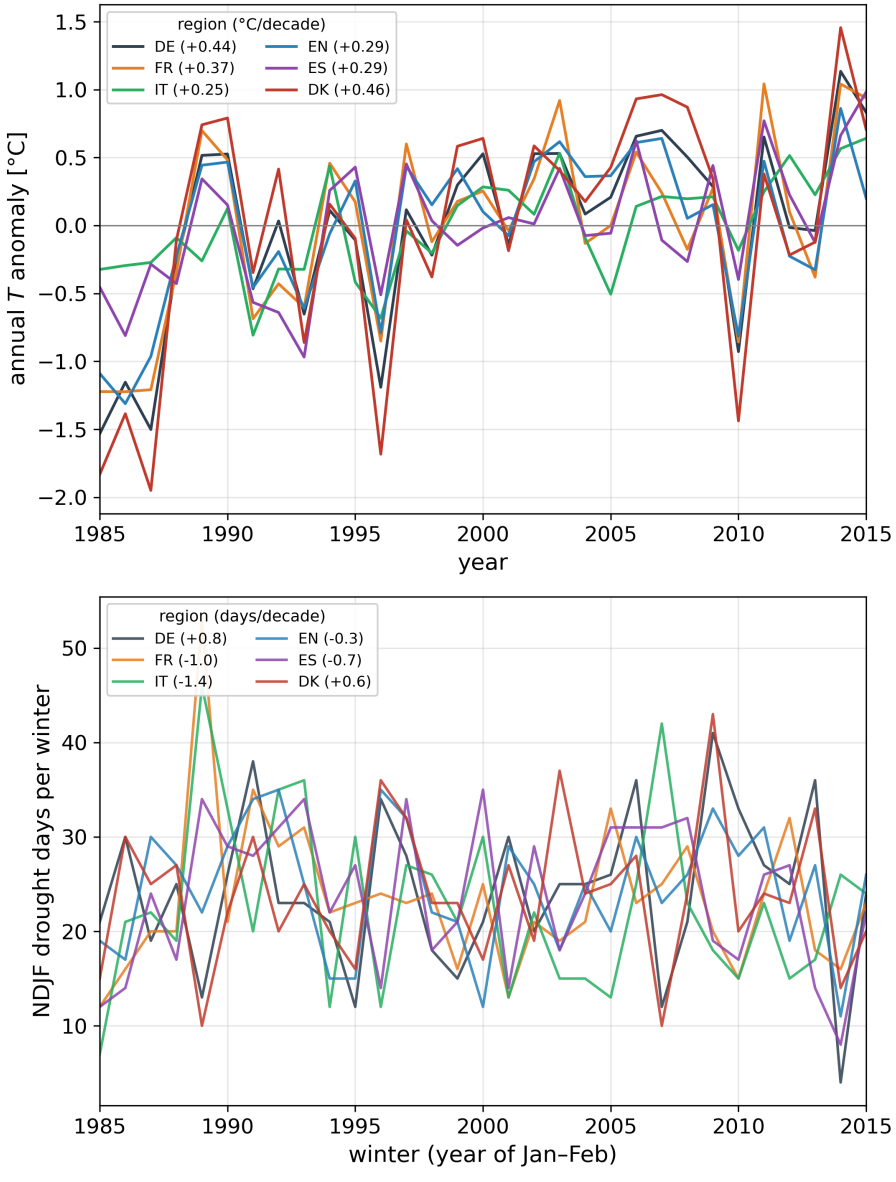



**Figure 2.** Modern-era temperature and winter wind-drought frequency by region. Top: annual ERA5 near-surface temperature anomaly. Bottom: number of NDJF wind-drought days per winter. Lines show the regional series; values in the keys give the corresponding decadal trends.

https://doi.org/10.5194/essd-2026-755
Preprint. Discussion started: 22 October 2026
© Author(s) 2026. CC BY 4.0 License.



Open Access Earth System Science Data Discussions

Beyond the early recovery, the modern part of Figure 3 shows the reconstruction tracking genuine large-scale variability rather than noise. Winter by winter over 1940–2015, the northern regions' mean wind follows the independent ERA5 record almost exactly (correlation $r = 0.99$). The clearest feature is the persistent positive phase of the North Atlantic Oscillation (NAO) through the late 1980s and 1990s (Hurrell, 1995). Northern winter wind rose about 5 % above its mid-century level, while the Mediterranean regions remained slightly below, producing a north–south dipole of about seven percentage points. ERA5 reproduces this swing to within a fraction of a percentage point: over 1981–2000, the northern excess is $+4.8\,\%$ in both records. The opposite signs in north and south are the recognised spatial signature of the NAO on western European winter wind speeds (Zubiate et al., 2017).

This is a low-frequency signal. The moving-window calibration (Sect. 6) deliberately removes such multidecadal variability from the released daily series, while retaining it in the raw (uncorrected) wind column of the released files and the optional low-frequency add-back (Sect. 9.3).

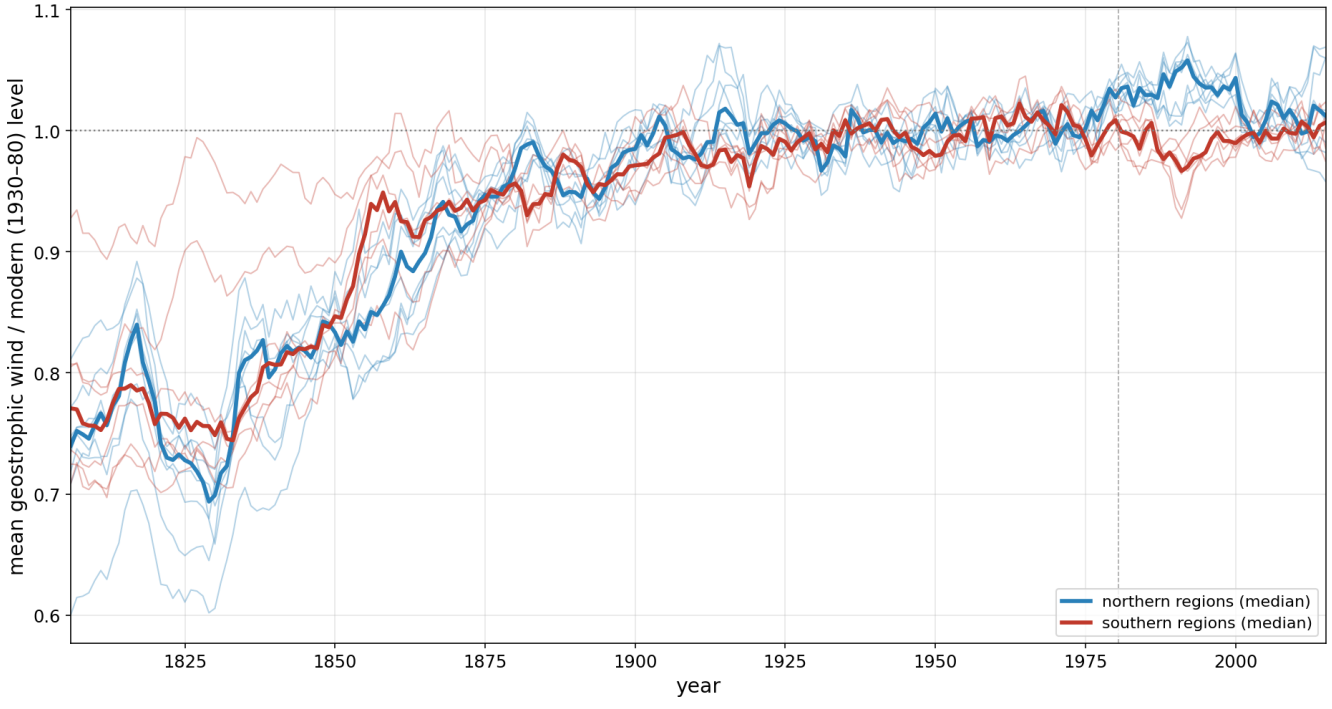



**Figure 3.** Mean reconstructed wind relative to each region's modern (1930–1980) level, at five-year resolution, 1806–2015, for the fourteen regions grouped into northern (blue) and southern (red) synoptic blocks. Thin lines are the individual regions (blue, north; red, south) and bold lines the block medians. The dashed vertical line marks the 1980/81 boundary between the two 20CRv3 production streams.

https://doi.org/10.5194/essd-2026-755
Preprint. Discussion started: 22 October 2026
© Author(s) 2026. CC BY 4.0 License.



Open Access Earth System Science Data Discussions

### 4.2 Test for an instrumental bias

The early deficit could arise either from residual barometer errors or from smoothing of the poorly constrained pressure field. These mechanisms have different signatures. An instrumental offset is additive, whereas ensemble smoothing reduces the pressure gradient approximately proportionally.

We compare the early (1806–1849) and well-observed (1930–1980) wind distributions with temperature-stratified quantile–quantile fits, $Q_{\mathrm{ref}} = a\,Q_{\mathrm{early}} + b$. The multiplicative component $(a-1)\,\mu$ dominates the bias in every region, while the additive component $b$ is small and often consistent with zero (42 of the 70 region–temperature bins; Table 4, Figure 4). Where its temperature dependence is significant, its slope is *negative*, from $-0.019$ (Romania) to $-0.137$ (Atlantic Iberia). This is the opposite sign to what a residual mercury-barometer error would leave. Historical mercury barometers over-read as they warm, so an incompletely corrected thermal-expansion error would raise the apparent pressure with temperature and give a positive slope. The intercept $b$ itself is a fragile extrapolation far below the weakest observed wind (adding a curvature term makes it grow and flip sign; Supplement), so the conclusion rests on the multiplicative term and the sign of the temperature slope, not on the value of $b$. We therefore attribute the dominant early bias to ensemble-mean smoothing rather than to an instrumental offset.

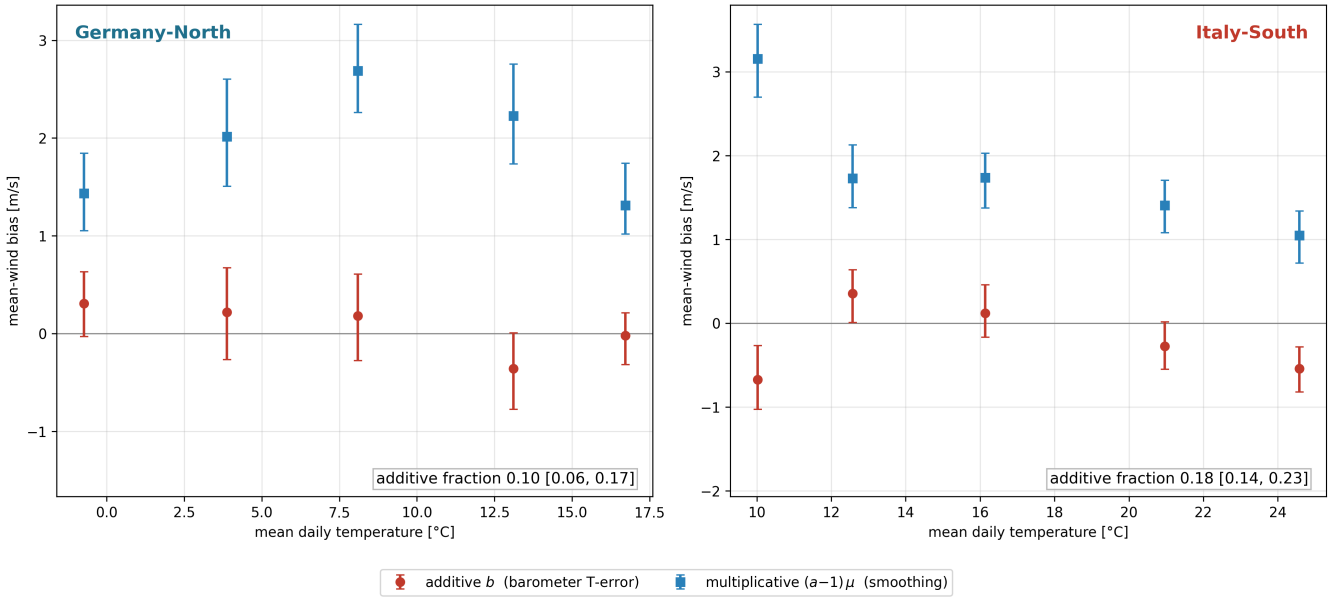



**Figure 4.** Decomposition of the early wind bias for northern Germany and southern Italy (Table 4). For each temperature bin the total bias between the early epoch (1806–1849) and the well-observed decades (1930–1980) is separated into an additive component ($b$, red) and a multiplicative component ($(a-1)\,\mu$, blue). Error bars are 95 % year-block-bootstrap intervals (500 resamples).

https://doi.org/10.5194/essd-2026-755
Preprint. Discussion started: 22 October 2026
© Author(s) 2026. CC BY 4.0 License.



Open Access Earth System Science Data Discussions

### 4.3 Ensemble-mean smoothing in the sparse-observation record

The observed bias is consistent with smoothing of the ensemble-mean pressure field when observations are sparse. 20CRv3 represents each day with an ensemble of eighty weather reconstructions, all constrained by the same assimilated pressure observations. Where those observations are sparse, the members differ in the position and amplitude of weather systems, so their mean smooths the pressure gradients and weakens the derived geostrophic wind. The effect is strongest early in the record and is approximately proportional to wind speed.

The interpretation is also consistent with the historical observing network. The wind bias decreases on the same timescale over which European surface-pressure observations become widespread (Figure 3).

### 4.4 Residual bias in the well-observed period

Throughout the analysis, 1930–1980 provides the well-observed reference period for the historical reconstruction. By then, the European observing network was essentially complete (Sect. 4.3), and the sparse early stage of the reconstruction had ended (Sect. 2.1). These decades therefore provide the internal reference for the correction. The procedure corrects changes in bias relative to 1930–1980; it cannot identify or remove a bias that was already present during the reference period. To find the residual bias, we compare our wind directly with ERA5 over their 1940–1980 overlap (ERA5 begins only in 1940, so this window is shorter than the 1930–1980 internal reference), on a matched scale and time basis. The old reconstruction still runs low by a few per cent in geographically flat regions and up to about a sixth in regions with strong channelling effects (Figure 6; Sect. 5). The quantiles of the raw reconstruction, plotted against the modern reference, fall along an almost straight line through the origin (Figure 5), indicating a proportional (scale-invariant) attenuation across all wind speeds.

For a line of the form $v_{\mathrm{ERA5}} = a\, v_{\mathrm{20CR}}$, the slope $a$ measures this attenuation, and the residual correction reported here, $100\,(1 - 1/a)$, is the percentage by which each region must be adjusted to reach the ERA5 level over 1940–1980 (Figure 6). A single parameter per region therefore describes the residual completely, and applying it is the second step of the correction (Sect. 6), which brings the well-observed level of the reconstruction into agreement with the modern reference. Leftover smoothing would attenuate strong winds more than weak ones and would curve this relationship; its observed linearity indicates that no such effect remains. In the dense modern network the ensemble members are in close agreement, leaving only a fixed scale factor between the coarse, pressure-derived wind and the modern reference, and this factor is essentially unchanged whether estimated near the middle of the century or in recent decades. The one-parameter residual assumes this linearity across the distribution; any curvature at the extreme upper tail (above the 95th percentile), where sub-grid channelling can respond nonlinearly, is not resolved by this step, a caveat for the rarest high-wind events, though the released product targets low-wind droughts and the primary quantile map of Sect. 6 follows the full distribution.

https://doi.org/10.5194/essd-2026-755
Preprint. Discussion started: 22 October 2026
© Author(s) 2026. CC BY 4.0 License.

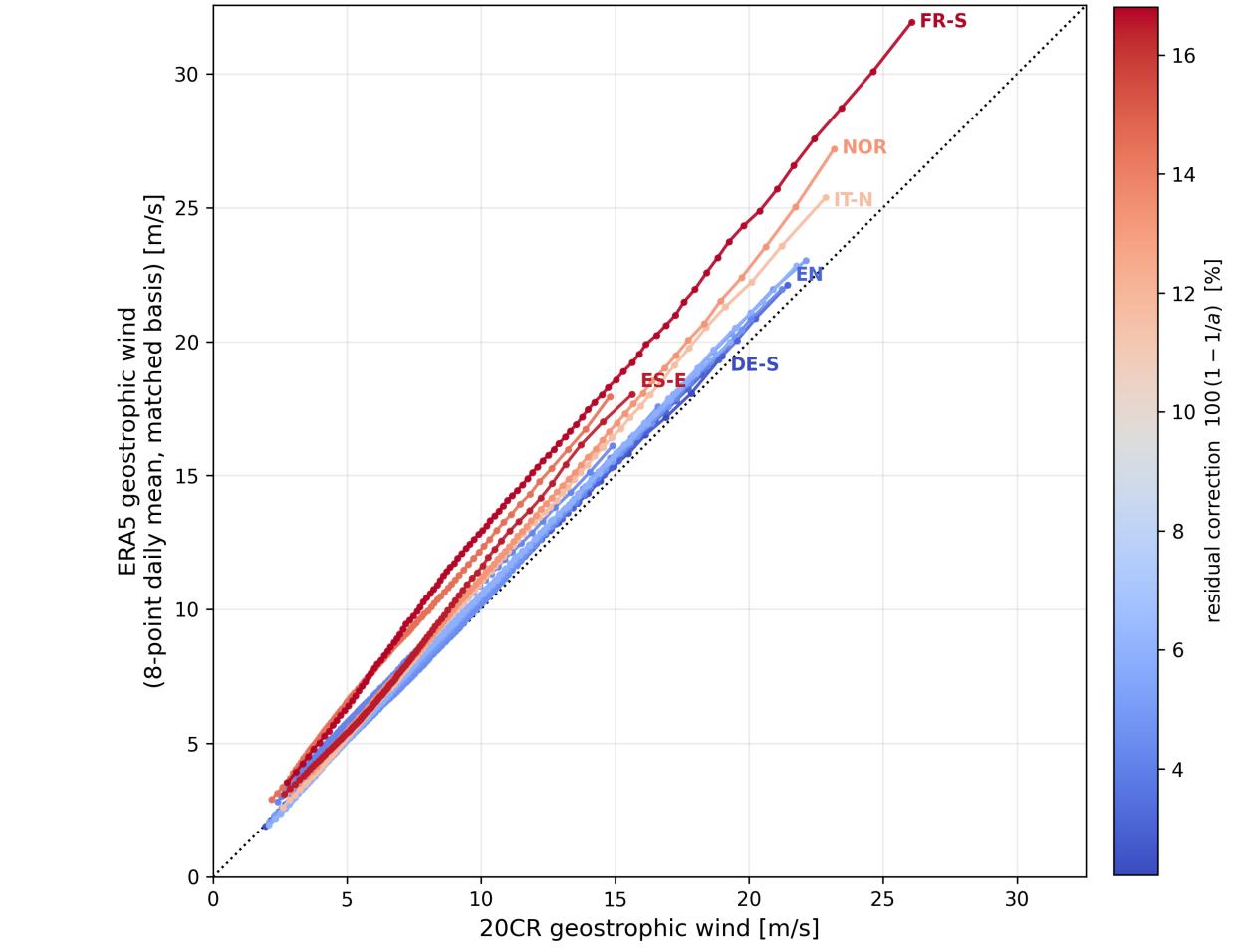



**Figure 5.** Residual bias in the well-observed decades, one line per region over the 1940–1980 overlap. Each line is a quantile–quantile relationship. At each cumulative probability the old wind is plotted against the modern one, both on the matched spatial scale and eight-point daily-mean basis (Sect. 2.6). Each line lies above the 1:1 diagonal, and its tilt is the region's residual correction (Figure 6). All fourteen regions are coloured by that correction (colour bar); for legibility only the outliers are labelled, the most-channelled (FR-S, ES-E, NOR, IT-N) and the flattest (DE-S, EN).

https://doi.org/10.5194/essd-2026-755
Preprint. Discussion started: 22 October 2026
© Author(s) 2026. CC BY 4.0 License.



Open Access Earth System Science Data Discussions

## 5 Spatial structure of the residual correction

The residual correction varies strongly between regions. It must be read on the matched eight-point basis (Sect. 2.6). A single-hour modern reference, for example at 12 UTC (noon), has a higher mean wind and would make the old record look about twice as deficient as it is. On that basis the correction runs from a few per cent to about a sixth, with a median of 5.6 % (against 10.8 % on the noon basis; Figure 6). It is smallest, and in three regions indistinguishable from zero, over flat, open terrain (southern Germany 2.0 %, England 2.9 %, southern Italy 4.0 %), and largest, 12–17 %, in five channelled regions, led by the Spanish Mediterranean (17.0 %) and the Rhône corridor (16.6 %), with Romania, southern Norway, and the Po basin completing the group.

The common factor is not elevation. Reanalyses struggle with complex terrain (Jiménez and Dudhia, 2010), and in these regions the orography channels much of the mean flow into a stream only a few tens of kilometres wide, at or below the roughly 100 km resolution, which the ensemble mean smears out, leaving the regional wind too weak. More elevated but less channelled regions need only a small correction, so the residual measures how much of a region's mean wind is carried below the roughly 100 km scale, not its elevation.

This shapes the dataset. Where a country spans two wind regimes, it is split in two (Sect. 4.2, Sect. 9). Four channelled regions (the Rhône corridor, Po basin, northern France, and southern Norway) carry a large, strongly seasonal correction and are calibrated season by season; the other ten use a single all-season map (Figure 18). The clean old-versus-modern relationship holds only at the roughly 100 km scale, which sets the method's natural resolution. Finer detail makes the pressure-derived wind noisy and, over mountains, contaminated by the sea-level reduction of station pressure, and belongs to the separate step that converts large-scale wind into wind-farm output.

**Seasonality of the residual correction.** The correction just described pools all months, which is safe only if it is the same in winter, the drought season, as in the annual average, and it mostly is. Re-measuring it season by season over the 1940–1980 overlap (Table 2; Figure 18) reveals a distinct seasonal winter residual in exactly the four channelled regions above (the Rhône corridor, the Po basin, northern France, and southern Norway), which are therefore calibrated with a separate quantile map for each of the four meteorological seasons (DJF, MAM, JJA, SON), so that every month is covered; the other ten keep a single all-season map. The winter-minus-summer swing runs both ways (the Mistral and the Scandinavian lee flows make winter the larger correction, whereas a weak summer thermal regime does so in northern France and the Po basin), and whether a region is calibrated per season is decided by this seasonal swing rather than by the overall size of its correction. The Spanish Mediterranean and Romania, for instance, carry large but permanently channelled corrections (the Cierzo down the Ebro, the Crivăț steered by the Carpathians) with almost no seasonal swing, and are therefore left pooled. Because each per-season map is a single monotone function within its season, it leaves the winter drought and persistence statistics unchanged (Sect. 6.3), as we confirmed directly.

https://doi.org/10.5194/essd-2026-755
Preprint. Discussion started: 22 October 2026
© Author(s) 2026. CC BY 4.0 License.

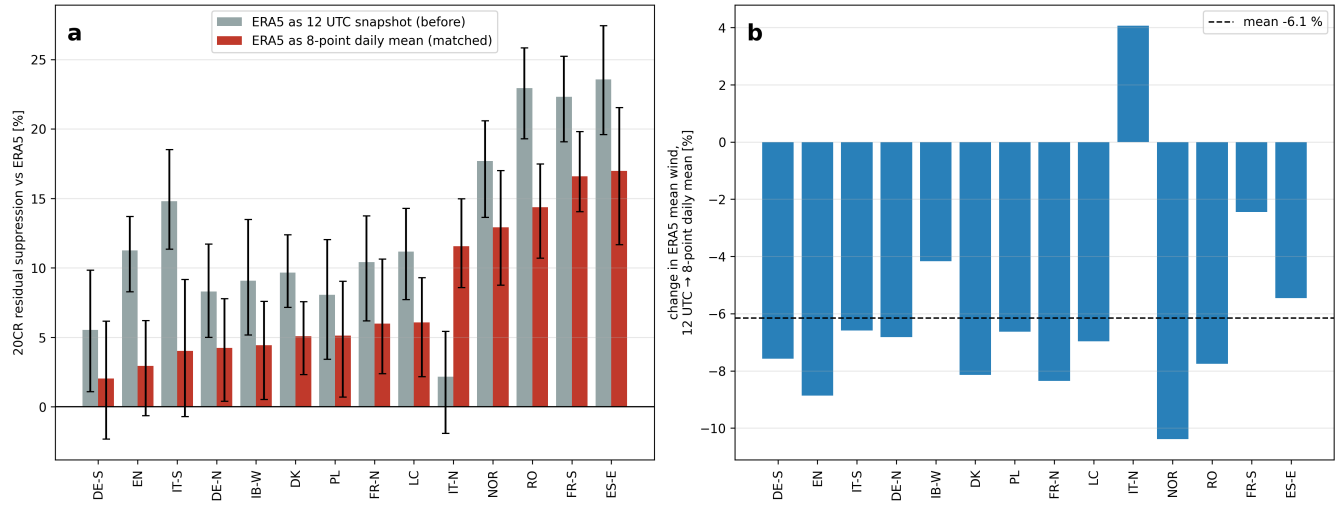



**Figure 6.** Residual wind correction for the fourteen regions. **a:** the per-region correction, sorted, estimated using a single 12 UTC ERA5 value (grey) and the matched eight-point daily mean (red; Sect. 2.6), with 95 % block-bootstrap intervals. **b:** the difference between the eight-point daily mean and the 12 UTC value of ERA5.

**Table 2.** Seasonal residual correction, per region. Residual correction (per cent) for the NDJF winter and JJA (June–August) summer over the 1940–1980 overlap, with the all-season value and the winter-minus-summer swing (percentage points). The four channelled-seasonal regions are calibrated per season, while every other region keeps a single all-season map (Sect. 6.1).

| Region | winter | summer | all | swing | calibration |
|---|---|---|---|---|---|
| Rhône (FR-S) | 20.4 | 9.4 | 16.6 | 11.0 | per season |
| Po basin (IT-N) | 5.1 | 14.0 | 11.6 | 9.0 | per season |
| N. France (FR-N) | 3.9 | 12.1 | 6.0 | 8.2 | per season |
| S. Norway (NOR) | 15.8 | 11.6 | 12.9 | 4.3 | per season |
| Sp. Med. (ES-E) | 14.1 | 13.6 | 17.0 | 0.5 | pooled |
| Romania (RO) | 14.5 | 14.9 | 14.4 | 0.4 | pooled |
| N. Germany (DE-N) | 4.6 | 4.8 | 4.2 | 0.1 | pooled |

https://doi.org/10.5194/essd-2026-755
Preprint. Discussion started: 22 October 2026
© Author(s) 2026. CC BY 4.0 License.

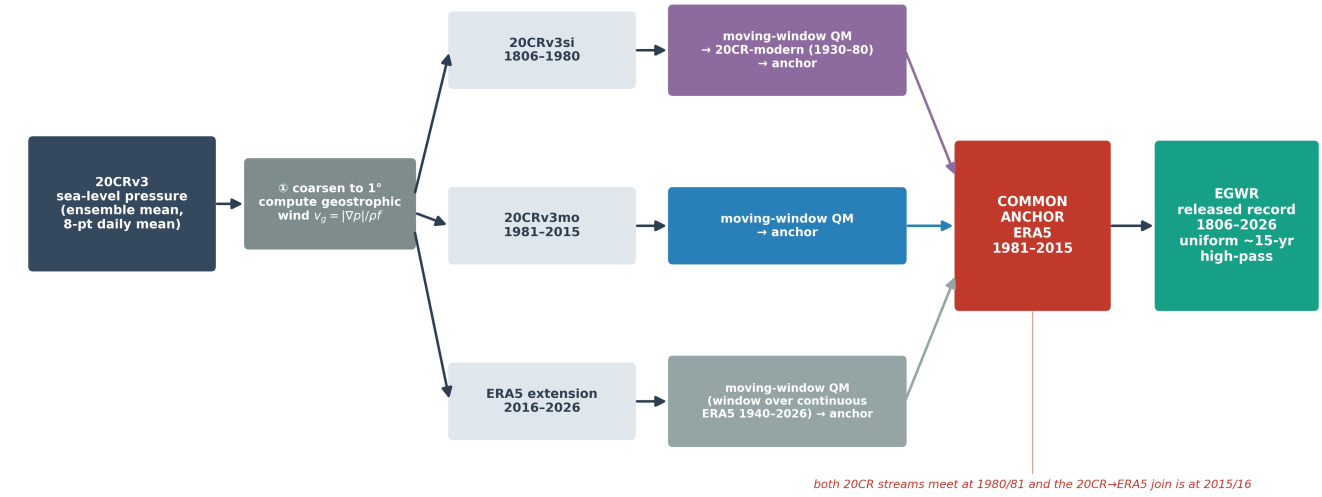



**Figure 7.** Workflow used to construct EGWR. Surface pressure from 20CRv3 is converted to regional geostrophic wind and corrected with a ±7-year moving-window quantile map referenced to a common ERA5 anchor. The two 20CRv3 production streams are corrected separately but mapped to the same reference; the 2016–2026 extension uses ERA5. All mappings preserve rank, so the timing of droughts is unchanged.

## 6 Correcting the record

The correction is applied region by region in two strictly monotonic, rank-preserving steps. First, a moving-window quantile map removes the time-varying smoothing bias by matching each period to the same reconstruction's well-observed 1930–1980 distribution (Sect. 6.1); this is the larger step. Second, a constant per-region correction aligns that distribution with the modern reference, ERA5 (Sect. 4.4). Neither step changes the ordering of daily winds (Sect. 6.3). The procedure is summarised in Figure 7.

### 6.1 Matching the distributions

For each region the historical wind distribution is mapped onto the reference distribution in a moving window of ±7 years (fifteen years). The value at each percentile of the historical distribution is replaced by the value at the same percentile of the reference distribution. The window lets the correction follow the gradual thickening of the observing network while avoiding abrupt jumps between fixed epochs. For 1806–1980, where ERA5 is unavailable, each window is mapped first onto the reconstruction's own well-observed 1930–1980 decades and then onto the common ERA5 anchor; for 1981–2015, where ERA5 overlaps, each window is mapped directly onto it. Because a moving window cannot span two different production systems, the two 20CRv3 streams are windowed separately on either side of their 1980/81 boundary; both still map onto the same ERA5 anchor, so the join carries no step. The 2016–2026 tail is ERA5 data, so its window runs over ERA5's own continuous 1940–

https://doi.org/10.5194/essd-2026-755
Preprint. Discussion started: 22 October 2026
© Author(s) 2026. CC BY 4.0 License.



Open Access Earth System Science Data Discussions

2026 record rather than over 20CR, which lets even the final years use a full, two-sided window. All mappings are monotonic and therefore preserve rank. Applied region by region, the mapping brings each old distribution onto the reference to within a Kolmogorov–Smirnov distance (the largest gap between two cumulative distributions) below 0.002 (from 0.05–0.27 before; Figure 8).

A fixed calibration does not account for the changing strength of the smoothing bias. Applying a static correction increases the apparent persistence of the early record. In the test shown here, the blocking-decay length (the characteristic timescale over which blocking-driven calm spells decay) changes from 1.95 to 2.50 days and the one-in-a-thousand-winter drought from 16.9 to 20.4 days. Coarser forty-year calibration epochs remove most of this difference; longer windows produce little further change.[1]

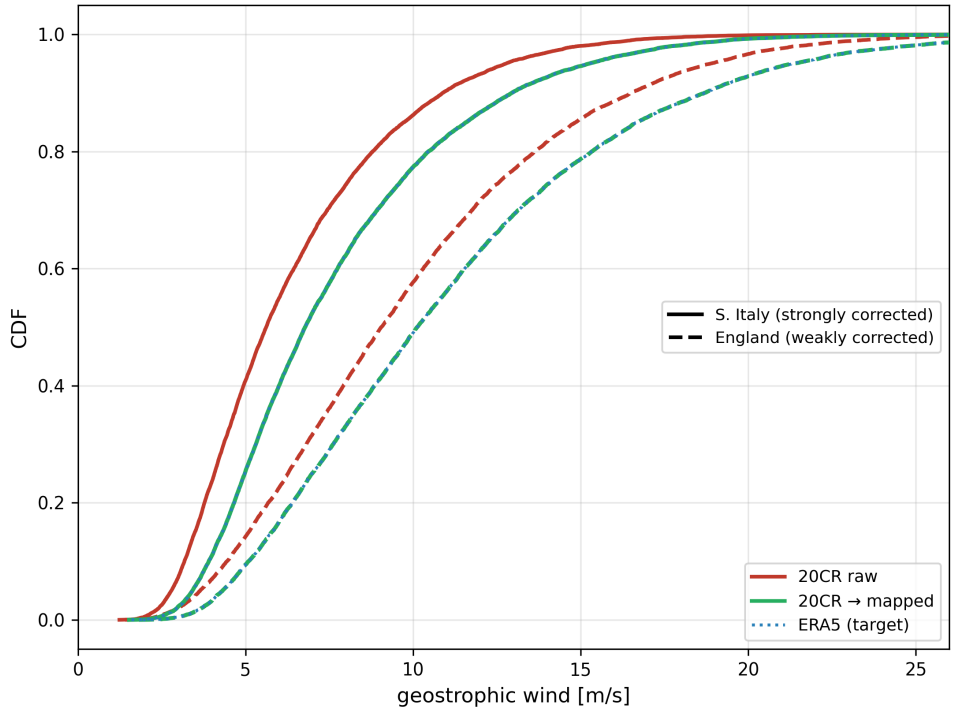
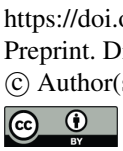



**Figure 8.** Quantile calibration, for a strongly corrected region (southern Italy, solid) and a weakly corrected one (England, dashed). Cumulative distributions of the daily geostrophic wind before (red, 20CR raw) and after (green, mapped onto the reference) calibration, with the ERA5 target as a dotted blue line. The mapped curve lands on the ERA5 target by construction; for England the dotted ERA5 line overlaps the dashed mapped curve.

[1]We tested other window resolutions (half-widths of ±5 and ±15 years, which bracket our canonical ±7-year window), and the record is robust to the choice. The fitted blocking-decay length shifts by under 0.06 days across this range.

https://doi.org/10.5194/essd-2026-755
Preprint. Discussion started: 22 October 2026
© Author(s) 2026. CC BY 4.0 License.



Open Access Earth System Science Data Discussions

### 6.2 Scope of the correction

The correction changes the amplitude of the wind, not its timing. The ensemble-mean smoothing of the sparse early fields (Sect. 4.3) weakened the wind and lost some day-level detail that no statistical correction can restore. It did not, however, scramble the sequence of weather. Over the overlap the raw reconstruction and ERA5 rise and fall together, with a same-day correlation that is high in every region ($r \gtrsim 0.95$; Figure 9). The historical reconstruction therefore preserves the timing of the large-scale evolution of calm and windy spells, even though sparse observations smooth some day-level detail; primarily their amplitude is too low, which is the situation the distribution correction is designed to address.

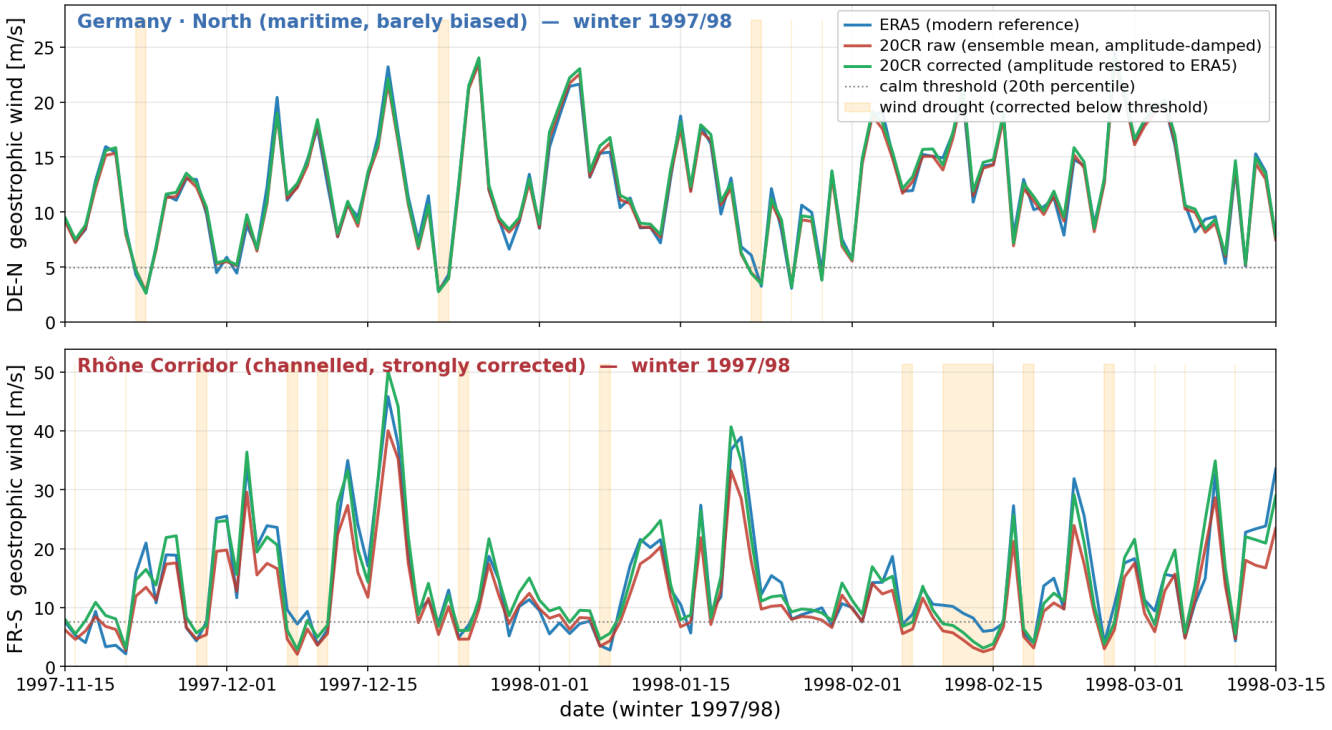



**Figure 9.** Daily wind during winter 1997/98 before and after calibration, for northern Germany (top) and the Rhône corridor (bottom). Raw 20CRv3 (red), corrected wind (green) and ERA5 (blue) are shown together; the dotted line marks the regional 20th-percentile threshold and shading identifies wind-drought days.

### 6.3 Preservation of event timing

Any statistic that depends only on the rank or temporal ordering of daily winds is therefore unaffected by the correction (Sect. 6.1). This includes the occurrence of relative-threshold droughts and the run structure of the calm spells, that is, the lengths of the consecutive below-threshold runs and how they cluster in time. We verify this directly by defining calm days

https://doi.org/10.5194/essd-2026-755
Preprint. Discussion started: 22 October 2026
© Author(s) 2026. CC BY 4.0 License.



Open Access Earth System Science Data Discussions

relative to each era's own distribution: drought duration and clustering remain stable across the record, apart from the earliest decades, where the sparse observing network affects drought frequency (Sects. 6.4–6.5).

### 6.4 The pre-1850 excess and the observing network

The earliest decades appear to have an elevated wind-drought rate. This feature can easily be misread as either a climatic signal or a reconstruction artefact. Read at face value across all fourteen regions, the pre-1850 winters appear to hold about 1.5 times as many long droughts (lasting ten days or more) as the modern era, a rate ratio of about 1.5. However, this figure is dominated by the regions that had almost no assimilated pressure observations at that time, and it largely reflects the observing network rather than the climate.

The apparent excess tracks the observing gaps, not the calendar. Region by region, the size of the early excess follows the early station density. Zones densely observed from the outset (Britain, Scandinavia, Denmark, northern Germany and the Po basin) show almost none of it (rate ratio $\approx 1.1$). In contrast, zones effectively blank until the mid-nineteenth century (Iberia, interior France, Poland, and the Balkans) carry essentially all of it (rate ratio $\gtrsim 1.9$). The two groups do not overlap, and their separation is statistically significant (Mann–Whitney $U$ test, $p = 0.006$). This is the drought counterpart of the mean-wind bias diagnosed in Sect. 4. The ensemble-mean smoothing of a sparse pressure field both weakens and over-clusters calm spells (Sect. 4.3). The excess is therefore not a climate result but a reliability one, and we handle it exactly as we handle the mean bias, with a per-region reliability start. The criterion that sets those starts, the reduction they achieve, the residual that remains, and the reduced confidence it leaves on the earliest decades' duration statistics are the subject of Sect. 6.5.

### 6.5 Region-specific recommended start years

The reliability of the reconstruction varies across Europe and over time. Rather than impose a single continental cut-off, we assign each region a recommended earliest year for quantitative extreme-value analysis. The start year is determined from the historical observing network and terrain alone, independently of the drought statistics.

For each decade we compute the mean distance from points within a region to the nearest assimilated pressure observation, and deem the region reliable once this distance falls below about 500 km, with the threshold tightened over rough terrain and relaxed over flat terrain (over flat terrain the pressure field decorrelates slowly, so a sparse, distant network still constrains it; over broken terrain it decorrelates quickly). The criterion is supported by the observed relation between observation coverage and retained day-to-day variance (Supplement, Fig. S10).

The resulting years are listed in Table 3 and shown region by region in Figure 1. The densely observed, largely flat regions of north-west and Central Europe (the British Isles, the Low Countries, northern and southern Germany, northern France, Denmark, and the Po basin) are reliable from the beginning of the record in 1806. Poland follows around 1815, the Rhône and southern France around 1835, Atlantic and Mediterranean Iberia and southern Italy around 1855, southern Norway around 1870, and Romania, the last-surveyed Balkan interior, around 1930. While the full 1806–2026 series is released for every region, the recommended start year denotes the threshold for quantitative event-value analysis; earlier decades remain available with diagnostic quality flags rather than being truncated. For the planned one-degree gridded product (Sect. 9),

https://doi.org/10.5194/essd-2026-755
Preprint. Discussion started: 22 October 2026
© Author(s) 2026. CC BY 4.0 License.



Open Access Earth System Science Data Discussions

the same coverage-and-terrain diagnostic becomes per-cell metadata, a `recommended_start_year` and a time-varying `reconstruction_confidence`, so that a user selects each cell's analysis window from the local network rather than applying a blanket rule.

**Table 3.** Recommended earliest year for quantitative extreme-value analysis, by region, from the terrain-modulated observation-coverage criterion. The full 1806–2026 reconstruction is released for all regions; the recommended start year indicates where earlier decades have reduced reliability.

| Start | Regions | Basis |
|---|---|---|
| 1806 | England, Low Countries, N. Germany, S. Germany, N. France, Po basin, Denmark | flat terrain and/or dense early network, long coherence scale |
| 1815 | Poland | flat, but a local observational gap until the 1810s |
| 1835 | Rhône / S. France | broken terrain; nearby network only from the 1830s |
| 1855 | Atlantic Iberia, Spanish Mediterranean, S. Italy | complex terrain; network reaches them mid-century |
| 1870 | S. Norway | mountainous and far from the early network |
| 1930 | Romania | Balkan interior, last-surveyed; adequate local coverage only in the 20th century |

The reliability horizon is statistic-dependent. The early network does not affect all aspects of the reconstruction equally. The amplitude correction restores the distribution of wind values but not the temporal autocorrelation the early smoothing alters, and ensemble agreement is poorer for individual short calm days but improves strongly with event duration (Figure 10; Supplement, Sect. S6). Persistent droughts are therefore better constrained than brief calms even in the sparse early record. We retain the full reconstruction but recommend the region-specific starts for quantitative event statistics.

Applying the region-specific starts substantially reduces the early excess. The pooled rate ratio for droughts lasting at least 10 days decreases from 1.50, when all regions are counted from 1806, to 1.16 when each region enters from its recommended start; for droughts of at least 8 days it likewise decreases from 1.44 to 1.16 (Figure 11). The remaining excess is small and cannot be separated from residual reconstruction uncertainty. Early long droughts occur slightly more often, but once a drought has reached 10 days its mean duration is essentially the same as in the modern record (mean-length ratio $\approx 0.99$).

None of the drought statistics depends on the earliest decades; the companion paper (Paul, submitted to *Nature Communications*) shows the fitted duration law is statistically unchanged whether the fit starts in 1806 or after 1850. One analysis deliberately retains the pre-1850 decades, the volcanic-response test of Sect. 10.1, where the early eruptions roughly double the observational sample of large tropical eruptions and are included explicitly, with their limits stated.

## 7 Validation against independent data

We validate the corrected record against three independent references, none of which were used to make the correction: the day-by-day overlap with ERA5 (Sect. 7.1), observed wind-power generation (Sect. 7.2), and two century-old anemometers (Sect. 7.3).

https://doi.org/10.5194/essd-2026-755
Preprint. Discussion started: 22 October 2026
© Author(s) 2026. CC BY 4.0 License.



Open Access Earth System Science Data Discussions

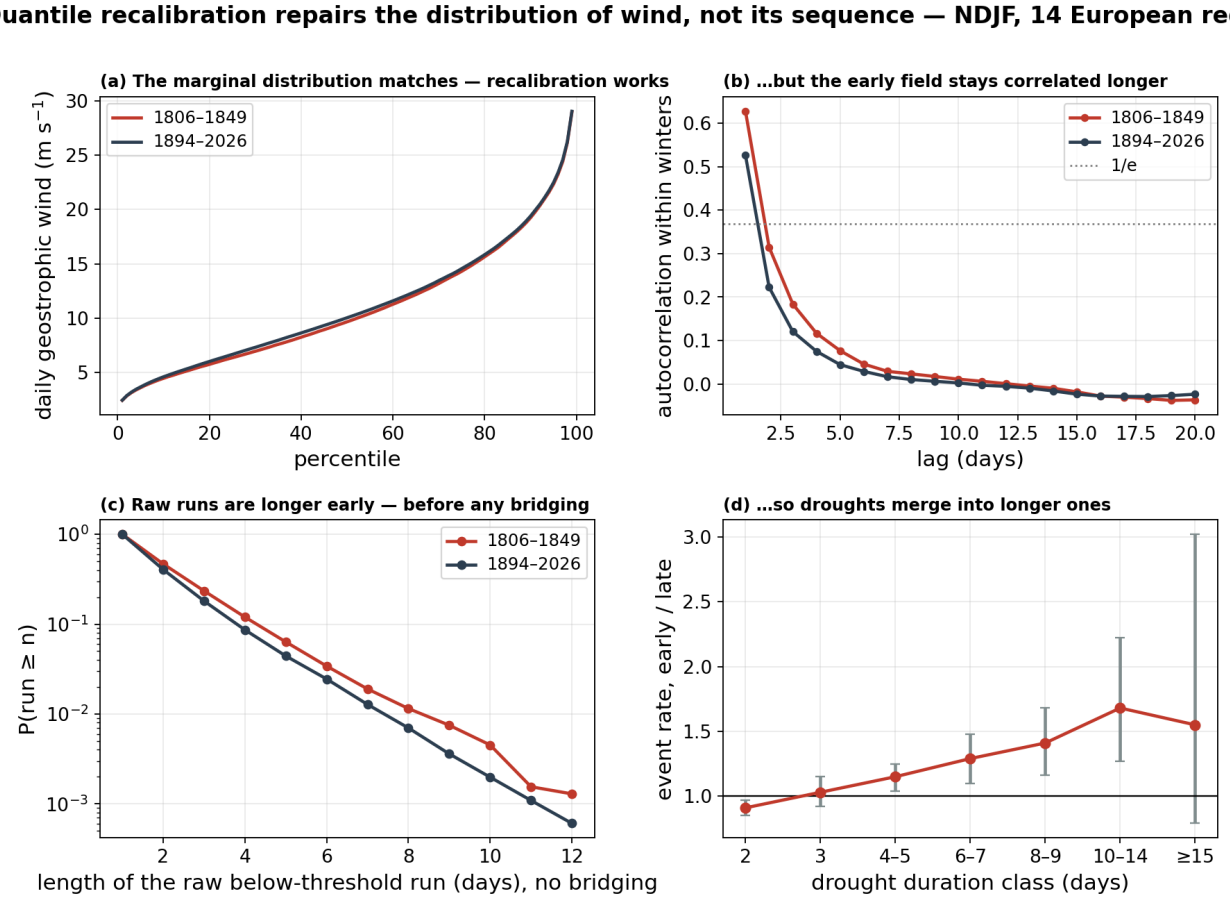



**Figure 10.** Early (1806–1849) versus modern (1894–2026) winter (NDJF) wind records, fourteen regions. **(a)** daily wind-percentile curves. **(b)** lag autocorrelation. **(c)** raw below-threshold run lengths (no bridging). **(d)** event-rate ratio by duration class.

### 7.1 Paired daily comparison with ERA5

The day-by-day comparison over the overlap period shows the effect of the correction directly. Before correction, the two records are closely correlated, but the historical reconstruction underestimates the largest values. In the paired daily comparison, the regression slope is 1.12 in the Rhône corridor and 1.03 in northern Germany (Figure 12, left). After calibration, the slopes are 0.93 and 0.99, respectively, while the close day-to-day correspondence with ERA5 is retained.

These paired daily slopes are not expected to equal the quantile-fitted slopes of Sect. 4.4. Because both variables contain day-to-day scatter, the paired regression slope is subject to regression attenuation and may fall slightly below one. The comparison therefore shows that the calibration removes the systematic amplitude bias without materially altering the day-to-day correspondence with ERA5.

https://doi.org/10.5194/essd-2026-755
Preprint. Discussion started: 22 October 2026
© Author(s) 2026. CC BY 4.0 License.

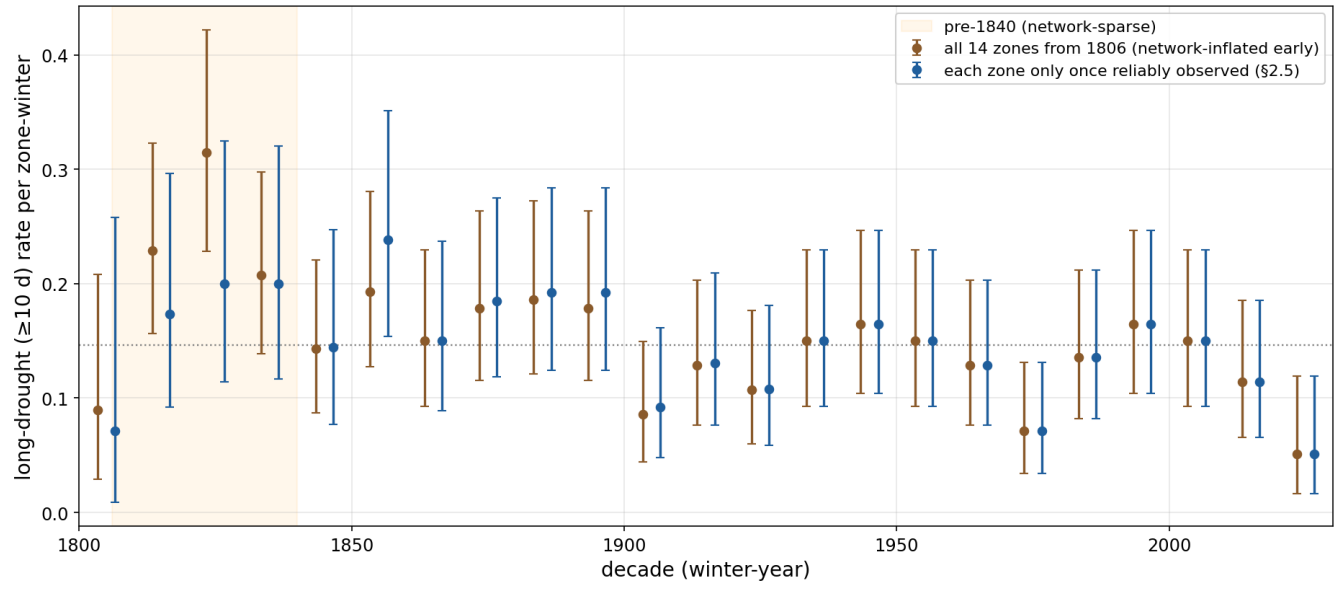



**Figure 11.** Rate of long wind droughts ($\geq$ 10 days) per zone-winter, by decade. Brown: all regions counted from 1806. Blue: each region counted from its recommended start year (Sect. 6.5; Figure 1). Error bars are 95 % Poisson intervals; the dotted line is the mean reliably-observed rate since 1850.

### 7.2 Comparison with observed wind generation

The record can also be evaluated against the observed capacity factor of the German wind fleet, derived from generation data reported on the German regulator's SMARD platform for 2015–2026 (Bundesnetzagentur, 2026). These observations are independent of the meteorological data used in the reanalyses and provide an established benchmark for evaluating reconstructed wind conditions (Staffell and Pfenninger, 2016). Over the overlap, the winter drought-duration distribution of the corrected record agrees with both ERA5 and the observed wind-power generation data within sampling uncertainty. Mean durations are 2.21 $\pm$ 0.05 d for the corrected record, 2.25 $\pm$ 0.09 d for ERA5, and 2.18 $\pm$ 0.15 d for the observed generation data (each $\pm$ one bootstrap standard error), while event rates are 8.12, 7.83, and 8.08 per winter, respectively. A Kolmogorov–Smirnov test between the corrected record and the observed generation data gives $D = 0.046$ and $p = 0.99$. With only a few hundred events, this large $p$ value indicates no evidence for a difference rather than proving that the distributions are identical. At the temporal resolution supported by the data, the three measures are statistically indistinguishable within their uncertainty.

This comparison provides an independent validation because the generation data represent the aggregate output of the operating German wind fleet rather than another meteorological reconstruction. The implications of the two-century record for the frequency of rare long droughts are developed in the companion paper (Paul, submitted to *Nature Communications*).

https://doi.org/10.5194/essd-2026-755
Preprint. Discussion started: 22 October 2026
© Author(s) 2026. CC BY 4.0 License.

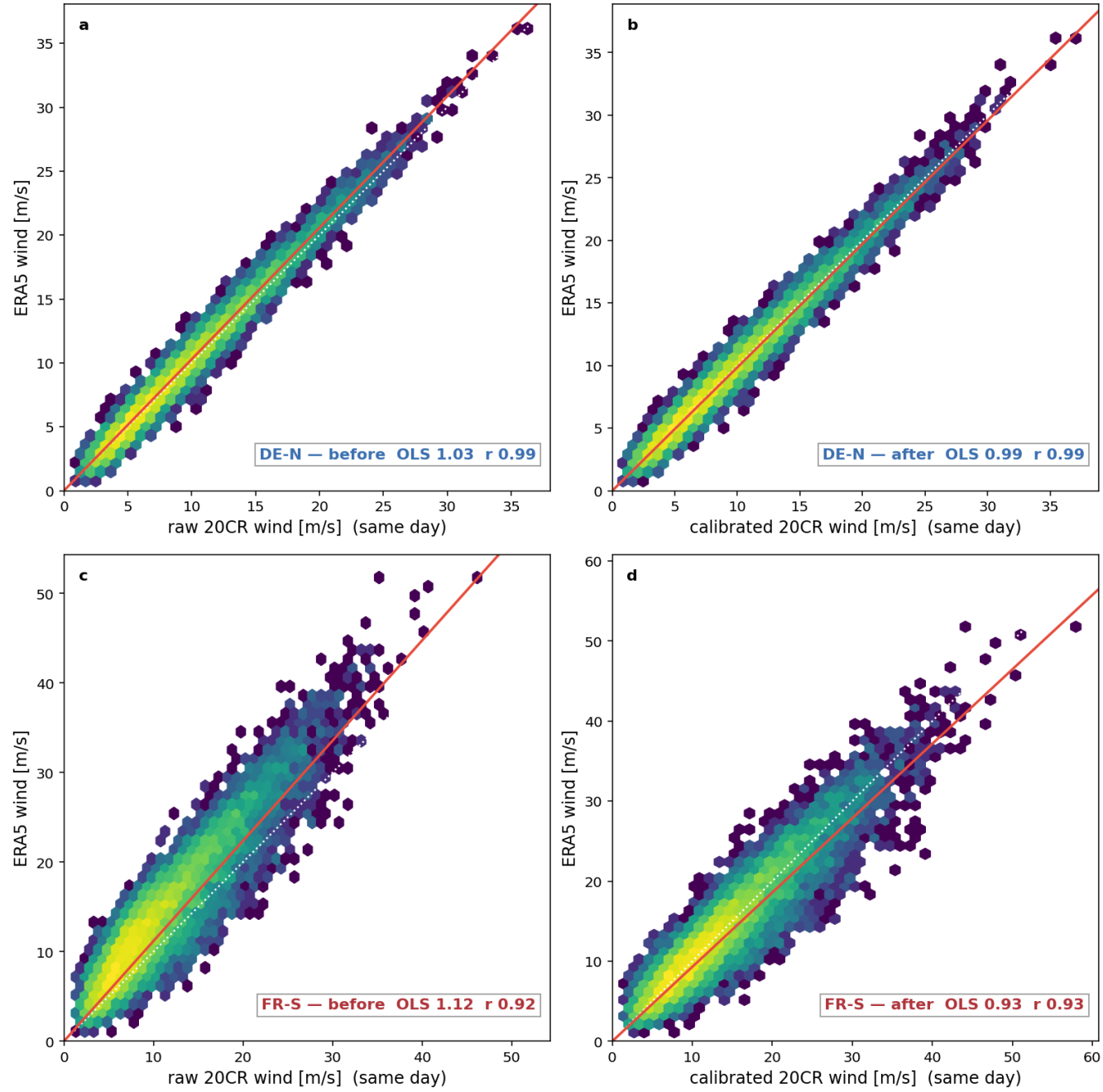



**Figure 12.** Daily 20CRv3 wind versus ERA5 before (**a**, **c**) and after (**b**, **d**) calibration, over the 1981–2015 overlap, for northern Germany (top) and the Rhône corridor (bottom). The red line is the ordinary regression through the daily pairs; the paired correlation is shown in each panel.

https://doi.org/10.5194/essd-2026-755
Preprint. Discussion started: 22 October 2026
© Author(s) 2026. CC BY 4.0 License.





### 7.3 Comparison with century-old anemometers

We also compare EGWR with long-term anemometer observations from Potsdam, Germany (since 1911; Deutscher Wetterdienst, 2026), and De Bilt, the Netherlands (since 1904; Koninklijk Nederlands Meteorologisch Instituut, 2026). These records extend into the period before modern reanalyses. Each anemometer measures wind at a single location, whereas EGWR represents large-scale wind derived from pressure. The comparison is therefore made at the synoptic, daily scale, at which both records respond to the passage of weather systems.

Annual averaging removes much of this shared day-to-day variability: the correlation is 0.28 at Potsdam and 0.10 at De Bilt, compared with daily correlations of 0.57 and 0.78, respectively (Figure 13). Over 1940–1980, when the anemometer records, EGWR, and ERA5 overlap, EGWR and ERA5 have nearly identical correlations with the observations: 0.57 and 0.58 at Potsdam, and 0.78 and 0.77 at De Bilt, respectively. At the synoptic scale, EGWR therefore agrees with these independent wind observations about as closely as ERA5 does. The stronger agreement at maritime De Bilt than at Potsdam is consistent with the greater influence of local surface conditions and topography on the latter.

## 8 Uncertainty and the reliability horizon

Reconstruction uncertainty is estimated from the spread of the eighty 20CRv3 ensemble members, with geostrophic wind computed independently for each. Because geostrophic wind depends on pressure gradients, spatially coherent differences between ensemble members largely cancel. Daily uncertainty is about 30 % in the sparse early record and falls to about 10 % by 2000; for seasonal means it is only a few per cent (Supplement, Sect. S6).

This uncertainty is correlated on synoptic timescales and therefore does not simply average out over a multi-day drought. In a noise-injection test, extra daily error is added to the corrected series and the duration law refitted; the fitted shape stays within its baseline uncertainty for injected errors up to about 30 %, which is comparable to the actual daily uncertainty of the early record. Only beyond that does the injected error become detectable, and it then shifts the estimate towards weaker persistence (Supplement, Fig. S15).

Reliability also depends on event duration. Persistent droughts are more consistently identified across ensemble members than individual short calm days, particularly in the early record. We therefore provide region-specific recommended start years for quantitative event statistics, based independently on the historical observing network and terrain rather than on the drought statistics themselves. Earlier years remain in the released product but are flagged as less reliable and shown as dashed in time-series figures (Supplement, Fig. S12).

## 9 The released dataset

Version 1.0 is released as fourteen validated regional series, each with an uncertainty estimate. A gridded one-degree field is planned as a subsequent product, after split-half reproducibility testing of the per-cell correction.

https://doi.org/10.5194/essd-2026-755
Preprint. Discussion started: 22 October 2026
© Author(s) 2026. CC BY 4.0 License.

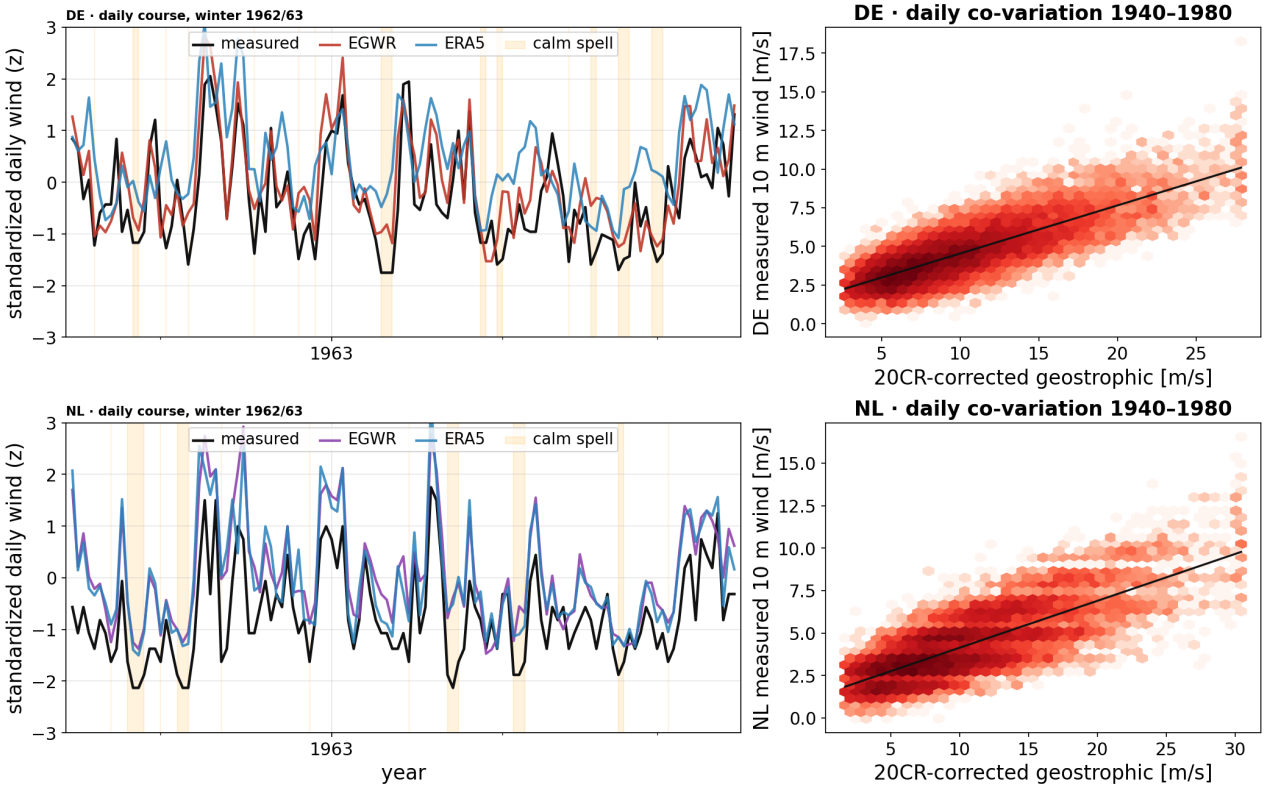



**Figure 13.** Daily wind at the Potsdam (top; DWD station 03987) and De Bilt (bottom; KNMI station 260) cup anemometers compared with the reconstruction and ERA5. In the legend, "measured" is the station 10 m wind, "EGWR" the 20CR-corrected geostrophic reconstruction, "ERA5" the modern reference, and "calm spell" marks days on which the measured wind is below its 20th percentile. *Left:* standardised daily series for the winter of 15 November 1962 to 15 March 1963 (the horizontal axis is labelled by year). *Right:* daily co-variation over the shared 1940–1980 period. All series are standardised (zero mean, unit variance over 1940–1980), so shapes and timing are comparable but absolute levels are not. Over 1940–1980 the daily correlations with the observations are 0.57 (Potsdam) and 0.78 (De Bilt) for the reconstruction and 0.58 and 0.77 for ERA5, whereas the annual-mean correlations are only 0.28 and 0.10.

https://doi.org/10.5194/essd-2026-755
Preprint. Discussion started: 22 October 2026
© Author(s) 2026. CC BY 4.0 License.





### 9.1 Regions and variables

The fourteen regions tile the one-degree grid without overlap (Figure 1), at the roughly 100 km scale on which the pressure-derived wind is robust (Sect. 5). A country is split where it spans distinct wind climates. Germany, France, Italy, and Iberia are each represented by two regions. Each released series carries, per day, the corrected geostrophic wind (m $s^{-1}$), the raw reconstructed wind, the correction factor, a source flag (which of the two 20CRv3 production streams, joined at the end of 1980, or the ERA5 extension), a per-epoch uncertainty, and a recommended start year. The full 1806–2026 series is released for every region; the recommended start year and quality flags mark the earlier, less-reliable years (Sect. 6.5, Sect. 8).

### 9.2 The 2016–2026 extension

Beyond 2015, the reconstruction is extended with ERA5 (flagged `ERA5`), high-passed in the same way against ERA5's record back to 1940. Both sides of the 2015/2016 join therefore have the same high-pass character. The scale-dependent 20CR–ERA5 transfer of Sect. 4.4 is applied at the 1980 stream boundary, not at this join. The remaining difference is therefore a small offset in mean level rather than a difference in distribution shape.

We remove this offset with a single shift for each region, matching 2016–2020 to 2011–2015 (median $-0.025$ m $s^{-1}$, reaching about $-0.3$ m $s^{-1}$ in the windiest northern regions). Because this adjustment is a constant shift, it preserves the rank ordering of days and therefore leaves relative-threshold statistics unchanged (Sect. 6.3). The unshifted ERA5 values remain available in the raw column.

### 9.3 Low-frequency add-back

The calibration removes variability on timescales longer than about fifteen years (Sect. 6; Figure 17). For applications that require absolute low-frequency levels, we therefore provide a separate ERA5-based add-back from 1940 onwards. It is intended for monthly-to-annual means rather than daily extremes, because the quantile correction is nonlinear. An independent 20CR-based estimate differs from the ERA5 component by a median root-mean-square (r.m.s.) difference of $0.07$ m $s^{-1}$ over 1940–2015. The pre-1979 component is less well constrained, and the add-back is undefined before 1940.

### 9.4 Uncertainty estimation

The per-value uncertainty combines three terms in quadrature, assuming they are independent (technical appendix): (i) the sampling error of the correction factor, from a block bootstrap over whole winters, small in well-observed epochs and growing backwards; (ii) the reanalysis's own ensemble spread, large where barometers were sparse; and (iii) a transfer error, measured by fitting to the 1940–1980 overlap and applying it to 1981–2015; the corrected mean then sits within about one per cent of the reference (median ratio 0.99, worst case 3 %). This combination is larger over complex terrain and in the nineteenth century, and it should be considered alongside the wind. At the two record ends (1806–1812 and 2020–2026) the moving window is one-sided and spans only seven to eight years rather than the full fifteen, roughly halving the sample and inflating term (i) by

https://doi.org/10.5194/essd-2026-755
Preprint. Discussion started: 22 October 2026
© Author(s) 2026. CC BY 4.0 License.

Open Access Earth System Science Data Discussions

about $\sqrt{2}$ and possibly introducing a small local phase or mean bias; the released uncertainty column carries this larger value and the per-timestep quality flag marks these boundary values.

### 9.5 Data formats, access, and licence

The regions are provided as CF-compliant NetCDF (one series per region) and CSV (one row per day), with the low-frequency add-back as a separate file. Each file carries a global attribute stating that variability slower than about fifteen years has been removed by design (so the series cannot be used to determine absolute multidecadal wind trends), and that the add-back restores absolute levels from 1940; a per-timestep quality flag identifies values within $\pm 7$ years of each record end (1806–1812, 2020–2026), where the one-sided window degrades the filter (Figure 17). Version 1.0 is deposited in a public long-term repository under CC-BY-4.0, with a reserved persistent DOI activated on publication, and is compatible with both upstream products (the U.S.-federal reconstruction, free with attribution; ERA5 under the Copernicus licence). The full processing chain (geostrophic derivation, moving-window quantile correction, ERA5 splice, and per-region build) is scripted and released, so the record can be regenerated from the public source reanalyses.

## 10 Usage examples

The long record supports analyses that the modern observational period constrains poorly. We give two examples: responses to explosive volcanic eruptions and to solar variability. Both are illustrative applications rather than formal attribution studies; in each, the value of the long record is that the larger sample narrows the statistical confidence intervals, and we report the resulting limits accordingly.

### 10.1 The response to volcanic forcing

We test the hypothesised increase in northern European winter wind following large tropical eruptions (Robock and Mao, 1992). Across the twenty-one eruptions of the record, we regress the standardised mean wind anomaly of the two following winters against the stratospheric sulfur injection ($\log_{10}$ VSSI; eVolv2k, Sigl and Toohey, 2024), separately for the northern and southern regions, with a Monte-Carlo permutation null.

Northern winter wind increases with eruption dose ($r = +0.61$, $p \approx 0.003$), whereas no corresponding relation is found in the south ($r = -0.10$, $p \approx 0.55$; Figure 14). The northern result is sample-limited and does not survive Benjamini–Hochberg false-discovery control across the family of region×lag×source-class tests, so we regard it as exploratory; wind-drought frequency itself shows no significant response. The example illustrates the additional constraint gained by extending the record to 1806.

### 10.2 Solar activity

We similarly test the eleven-year solar cycle using the sunspot number and related solar and heliospheric indices. None shows a significant regional wind or drought response. The largest effect is a one-to-two percentage point modulation of northern winter drought frequency, which is not significant. The high-pass character of the released series also limits the analysis to variability

https://doi.org/10.5194/essd-2026-755
Preprint. Discussion started: 22 October 2026
© Author(s) 2026. CC BY 4.0 License.

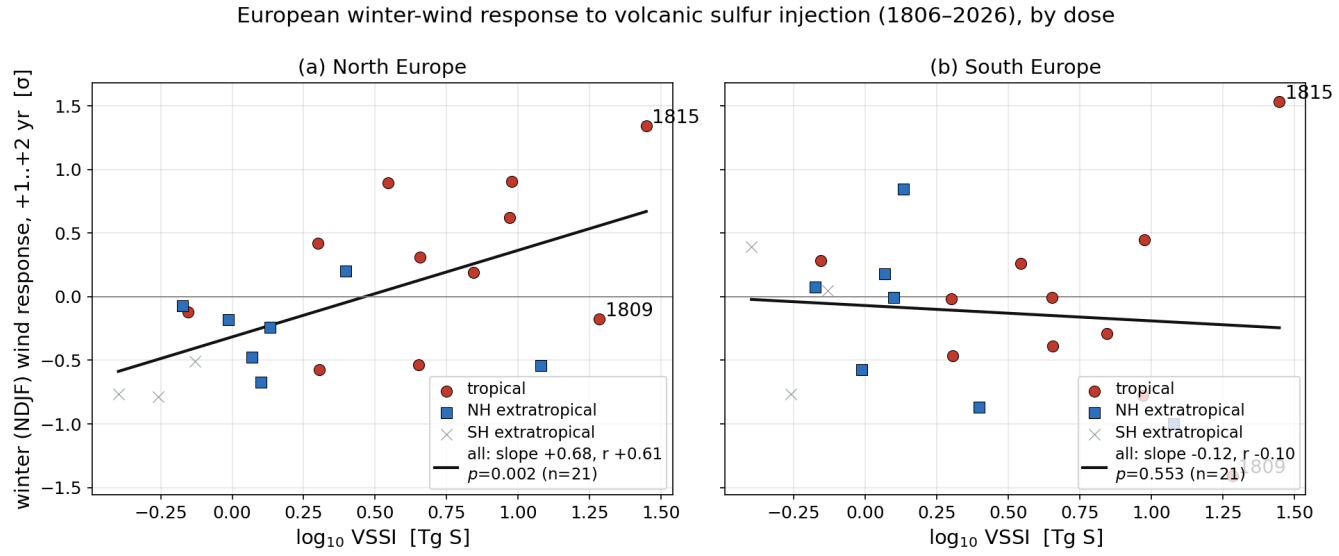



**Figure 14.** European winter (NDJF) wind response to volcanic sulfur injection, 1806–2026. For each of the twenty-one eruptions, the standardised mean wind anomaly of the two following winters against the eruption's stratospheric sulfur injection ($\log_{10}$ VSSI), for **(a)** the northern and **(b)** the southern regions. Symbols mark the source latitude (tropical, NH-extratropical, SH-extratropical); the solid line is the all-eruption regression (Sect. 10.1).

on timescales shorter than about fifteen years. EGWR therefore provides an empirical constraint on any solar modulation of European winter drought, but does not reveal a significant signal.

### 10.3 Statistical value of the long record

The practical value of the long record is statistical. Pooled across the fourteen regions, the released record provides 2721 zone-winters and 14 944 events, against 560 zone-winters for the last forty winters and 154 for the eleven winters of the observed-generation era (Figure 15). The three samples agree within uncertainty up to about twelve days, but the uncertainty of the short records increases rapidly beyond that. The long record therefore does not systematically change the estimated distribution. It constrains the rare-event tail much more tightly. The return levels this makes possible, and their bearing on energy adequacy, are developed in the companion paper (Paul, submitted to *Nature Communications*).

## 11 Limitations

EGWR provides large-scale geostrophic wind at daily and approximately 100 km resolution; it is not a reconstruction of local or hub-height wind. Four limitations are particularly relevant.

https://doi.org/10.5194/essd-2026-755
Preprint. Discussion started: 22 October 2026
© Author(s) 2026. CC BY 4.0 License.

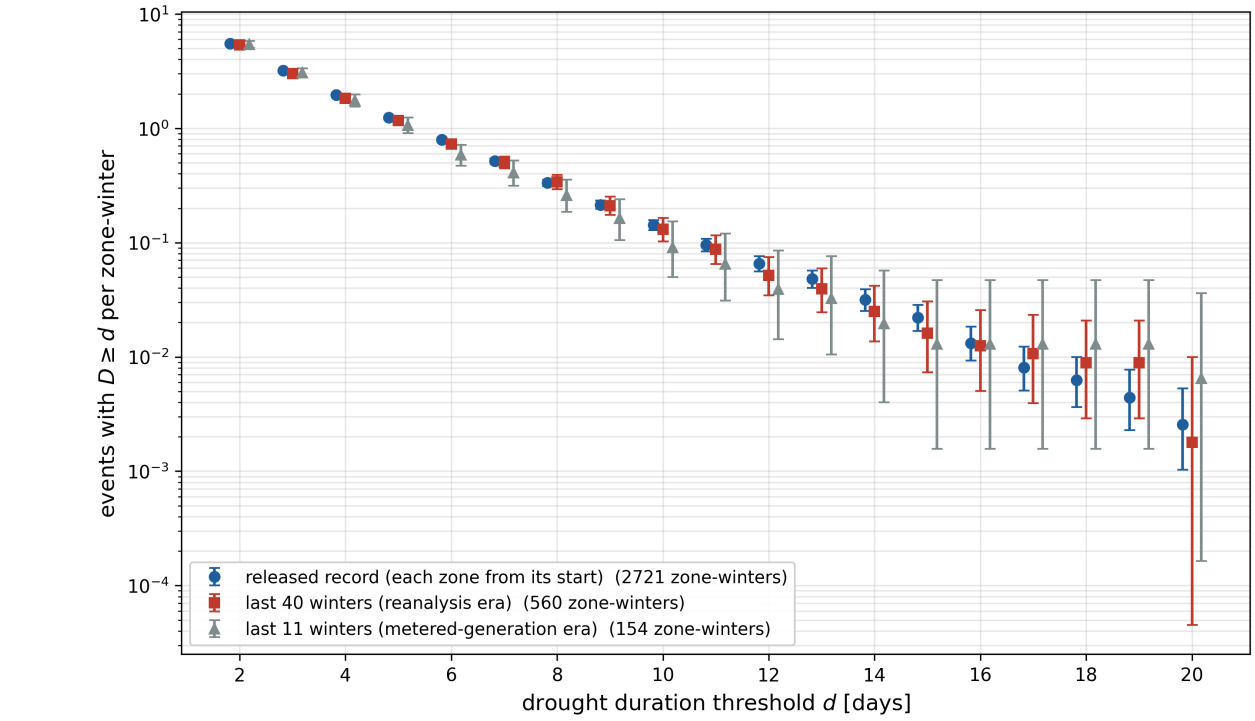



**Figure 15.** Wind-drought exceedance rate per zone-winter against the duration threshold, pooled over the fourteen regions, for three sampling windows: the full released record (each region from its recommended start), the last forty winters, and the last eleven. Error bars are exact 95 % Poisson intervals; points are offset horizontally for legibility.

1. The product represents the large-scale pressure-gradient wind, not near-surface or turbine-level wind. Conversion to wind power requires a separate, site-specific model.
2. Daily resolution does not resolve sub-daily variability or local thermally driven circulations.
3. The moving-window calibration removes variability on timescales longer than about fifteen years. The released series should therefore not be used to infer absolute multidecadal wind trends. The optional ERA5-based low-frequency diagnostic (Sect. 9) restores absolute levels from 1940 onwards.
4. The earliest decades have reduced reliability for persistence statistics. The amplitude correction restores the distribution of wind values but cannot recover the day-level detail smoothed out by sparse observations. Region-specific recommended start years identify the period suitable for quantitative event statistics; earlier values remain available with quality flags.

The correction also assumes that the ordinary daily wind distribution is approximately stationary. Modern observations show no significant regional trend, but this assumption cannot be tested directly in the early record. Within these limits, EGWR provides a homogeneous long-term baseline for large-scale European wind variability and persistence.

https://doi.org/10.5194/essd-2026-755
Preprint. Discussion started: 22 October 2026
© Author(s) 2026. CC BY 4.0 License.





## 12 Data availability

Version 1.0 of the EGWR, which provides the daily corrected geostrophic wind, along with per-region uncertainty and quality flags, for the fourteen reference regions between 1806 and 2026, is deposited in a public long-term repository under a Creative Commons Attribution licence (CC BY 4.0) and is cited as Paul (2026b). The dataset is archived at PANGAEA; its persistent identifier, 10.1594/PANGAEA.997348, is activated on publication of the dataset. During peer review and the public discussion the data are accessible at the PANGAEA landing page https://doi.pangaea.de/10.1594/PANGAEA.997348 and, without registration, through the review link https://www.pangaea.de/tok/53858500df139169fb9b2efa923acb07f6db0741. The optional low-frequency add-back file is included as a separately labelled diagnostic (Sect. 9). The upstream inputs are openly available: the NOAA/PSL 20CRv3 reanalysis and its assimilated observation counts (in the public domain with attribution), and the Copernicus Climate Change Service (C3S) ERA5 reanalysis (under the Copernicus licence). The released product is a modified derivative of both, as recorded in its metadata (Sect. 9).

## 13 Code availability

All Python scripts used for data processing (geostrophic wind computation, sliding-window quantile calibration, validation, and figure generation) are deposited with the paper under the MIT licence and are cited as Paul (2026a), with the persistent DOI `https://doi.org/10.5281/zenodo.22669767`. The deposited scripts reproduce the released series and every figure in this paper from the openly available inputs, so that an editor or reviewer can inspect and rerun the exact code that produced the reported results (see the statement on the use of generative AI in the Acknowledgements).

## 14 Author contributions

SP conceived and designed the study, developed and evaluated the methodology, performed the analyses and data processing, prepared the dataset and figures, and wrote the manuscript.

## 15 Competing interests

The author declares that he has no conflict of interest.

## 16 Acknowledgements

The author thanks Gil Compo (CIRES, University of Colorado Boulder) for his support in accessing details of the Twentieth Century Reanalysis (20CR) data.

**Use of generative AI.** Generative AI tools, including Claude (Anthropic), ChatGPT (OpenAI), and Gemini (Google), were used during the development of this work to assist with programming, checking calculations and reasoning, and improving the

https://doi.org/10.5194/essd-2026-755
Preprint. Discussion started: 22 October 2026
© Author(s) 2026. CC BY 4.0 License.



Open Access Earth System Science Data Discussions

clarity and structure of the manuscript. All analyses, scientific interpretations, and conclusions were independently evaluated and verified by the author, who takes full responsibility for the work. The author appreciates the intensive scientific discussions with the AI systems used during this work and the rapid access to data and information facilitated by Claude.

## 17 Technical methods

**Source data.** The long reconstruction is based on the NOAA-CIRES-DOE Twentieth Century Reanalysis version 3 (20CRv3; Slivinski et al., 2019; Compo et al., 2011), from which daily ensemble-mean sea-level pressure and 2 m temperature are used for 1806–2015. The record comprises two internally consistent production streams separated at 1980/81, accessed via OPeNDAP. The assimilated inputs are the corrected historical pressures of the International Surface Pressure Databank (Cram et al., 2015) and the ACRE data-rescue initiative. ERA5 (Hersbach et al., 2020; 1940–2026) provides the modern reference. Mean sea-level pressure and 2 m temperature are taken as eight-point daily means (Sect. 2.6) rather than values at a single hour.

**Geostrophic wind.** For each region and day we compute the geostrophic wind speed from the horizontal sea-level-pressure gradient using Eq. 1 (Sect. 2.3), with the symbols defined there. Temperature does not enter this expression. The geostrophic wind is set by the pressure gradient alone (the temperature gradient governs only the vertical shear of the geostrophic wind, the thermal wind, which is not used here). The pressure gradient is calculated by finite differences on the grid, with the zonal spacing adjusted by the cosine of latitude, and is then averaged over each regional box. Both records are evaluated at about $1^\circ$ resolution, with ERA5 coarsened to match. The gradient is calculated before spatial averaging because reversing this order would smooth the pressure field before differentiating it. The bias correction of Sect. 6 is applied to this derived box-mean wind, not to the pressure field, which avoids imposing a non-physical adjustment on the gradient across neighbouring grid cells.

**Annual means and anomalies.** The daily value **of the temperature**, $T_i(d)$, is the box-mean 2 m temperature over region $i$; the daily value **of the wind**, $v_i(d) = |\nabla p_i(d)|/(\rho f_i)$, is the box-mean geostrophic wind, taken from 20CR after bias correction. Both records are read on the same time basis, in the sense set out in Sect. 2.6. A day is the mean of the sub-daily analyses, the averaging being applied to the field (temperature, or sea-level pressure) before the derived quantity is formed. For 20CR this is what the archive supplies (the daily-mean `air.2m` and `prmsl` fields, each an average of eight three-hourly analyses); for ERA5 we construct the same thing from its sub-daily fields rather than reading a single hour. As Sect. 2.6 explains, this matters when the two records are compared in *level*. A single-hour ERA5 field yields a mean geostrophic wind about eight per cent higher than the eight-point daily mean. It does not matter for statistics defined relative to each series' own distribution, which are invariant to the choice. For region $i$ and year $y$ the annual means are the calendar-year averages of these daily values,

$$\bar{T}_i(y) = \frac{1}{N_y}\sum_{d\in y} T_i(d), \qquad \bar{v}_i(y) = \frac{1}{N_y}\sum_{d\in y} v_i(d), \tag{2}$$

with $N_y$ the number of days in the year. The temperature change is referenced to each region's own early baseline, $\Delta T_i(y) = \bar{T}_i(y) - \langle \bar{T}_i \rangle_{1806\text{–}10}$; the wind is expressed as a normalized anomaly relative to the 1940–1980 mean, $w_i(y) = \big(\bar{v}_i(y)/\langle \bar{v}_i \rangle_{1940\text{–}80} - 1\big) \times 100\%$. ERA5 is placed on the same baseline through the 1940–1980 overlap. The temperature anomaly defined here is what

https://doi.org/10.5194/essd-2026-755
Preprint. Discussion started: 22 October 2026
© Author(s) 2026. CC BY 4.0 License.



Open Access Earth System Science Data Discussions

Figure 2 plots; a running mean would introduce spurious multi-year pseudo-cycles (the Slutsky–Yule effect), so no temporal smoothing is applied to any of these series.

**Table 4.** The barometer test, per region. (main-text Sect. 4.2). For each region: the *additive fraction* of the mean-wind bias left to the intercept $b$ (95 % year-block-bootstrap CI); the temperature slope $\mathrm{d}b/\mathrm{d}T$ of that intercept ($\pm1$ standard error); the mean multiplicative component $(a-1)\mu$; and the number of temperature bins (of five) in which $b$ differs from zero. The multiplicative component carries essentially the whole bias (between one and four metres per second everywhere); the additive fraction is at most about a third, and where $\mathrm{d}b/\mathrm{d}T$ differs from zero it is *negative*, the opposite of a mercury-correction signature.

| Region | additive fraction [95 % CI] | $\mathrm{d}b/\mathrm{d}T$ [m s$^{-1}$ K$^{-1}$] | mean $(a-1)\mu$ [m s$^{-1}$] | bins with $b \neq 0$ |
|---|---|---|---|---|
| NOR | 0.22 [0.16, 0.27] | $+0.011 \pm 0.019$ | +3.09 | 5 of 5 |
| DK | 0.08 [0.05, 0.15] | $-0.037 \pm 0.015$ | +2.64 | 0 of 5 |
| DE-N | 0.10 [0.06, 0.17] | $-0.024 \pm 0.012$ | +1.94 | 0 of 5 |
| PL | 0.17 [0.11, 0.26] | $-0.032 \pm 0.010$ | +1.66 | 2 of 5 |
| EN | 0.10 [0.07, 0.15] | $-0.021 \pm 0.026$ | +3.66 | 3 of 5 |
| LC | 0.05 [0.04, 0.15] | $+0.000 \pm 0.015$ | +2.00 | 0 of 5 |
| DE-S | 0.07 [0.05, 0.16] | $-0.010 \pm 0.009$ | +1.55 | 0 of 5 |
| FR-N | 0.35 [0.25, 0.45] | $+0.008 \pm 0.011$ | +1.04 | 4 of 5 |
| IT-N | 0.31 [0.23, 0.45] | $-0.060 \pm 0.017$ | +0.96 | 1 of 5 |
| RO | 0.19 [0.15, 0.22] | $-0.019 \pm 0.010$ | +2.21 | 3 of 5 |
| FR-S | 0.22 [0.17, 0.26] | $-0.052 \pm 0.022$ | +2.49 | 2 of 5 |
| IB-W | 0.18 [0.14, 0.23] | $-0.137 \pm 0.021$ | +3.06 | 2 of 5 |
| ES-E | 0.20 [0.16, 0.25] | $-0.110 \pm 0.018$ | +2.05 | 3 of 5 |
| IT-S | 0.18 [0.14, 0.23] | $-0.030 \pm 0.013$ | +1.81 | 3 of 5 |

**Estimating and applying the correction.** For each region, the bias is measured by comparing wind *distributions* rather than individual days, through the quantile map of Sect. 6.1. This map is not fixed for the whole record. It is re-estimated in a window of about fifteen years ($\pm7$ yr) that slides along the record, so the correction follows the thickening of the observing network smoothly instead of jumping between fixed epochs. The *same* moving-window map is applied uniformly to all three sources (the two 20CR streams and the ERA5 extension), and every window is referenced to a single common modern anchor, ERA5 over 1981–2015. The two 20CR streams are calibrated separately across their 1980 boundary, because a moving window cannot straddle two different assimilation systems, but both are mapped to the same anchor, so no step is introduced there. The ERA5 extension is calibrated against ERA5's continuous record back to 1940, avoiding an edge artefact from its shorter extension period. Before 1940, where ERA5 is unavailable, each window is first mapped to the reconstruction's well-observed reference period (1930–1980) and then to the common anchor. Both maps preserve rank.

**Transfer function of the correction.** Because each moving window is mapped to a common anchor, the correction removes variability on timescales longer than the window while preserving shorter variations. We quantify this behaviour by injecting known low-frequency signals into the already-corrected, stationary series and applying the same moving-window correction again (Figure 17). The injected signal therefore enters before the correction is applied.

https://doi.org/10.5194/essd-2026-755
Preprint. Discussion started: 22 October 2026
© Author(s) 2026. CC BY 4.0 License.





The gain remains close to unity for periods up to about fifteen years, falls to one-half near twenty-five years, and below one-tenth by sixty years. Across the fourteen regions, the interquartile spread of the gain is below 0.002, showing that the response is determined primarily by the window rather than by the region. Injected amplitudes of 0.2, 0.5, and 1.0 m $s^{-1}$ produce gain curves agreeing within 0.012, indicating that the response is effectively linear over this range.

The correction also suppresses non-periodic low-frequency signals. An injected 1 m $s^{-1}$ step decays to zero residual within about thirty years, and a linear ramp leaves a mean residual of only 0.003 m $s^{-1}$. The correction therefore removes both persistent offsets and trends, rather than only long-period oscillations. Its response is degraded within $\pm 7$ years of each record end, where the window becomes one-sided; these years are flagged in the released files.

Because quantile mapping is formally nonlinear, the reported response is an empirical effective transfer function rather than a strict linear filter. The amplitude test shows that it is effectively independent of amplitude over the range examined. The released record is therefore suited to interannual and sub-decadal variability and to wind-drought statistics, but not to applications requiring absolute multidecadal levels or trends (Sect. 11).

**Optional low-frequency add-back, and its uncertainty.** For users who need absolute modern wind levels rather than the high-passed series, we supply the low-frequency component the filter removes. For each region this is the ERA5 box-mean geostrophic wind expressed as an annual anomaly relative to the 1981–2015 mean and smoothed with the same $\pm 7$-year window, 1940–2026. Added back to the released series it restores the slow variation of the level. There are two reasons it is a diagnostic rather than a validated field. First, the high-pass is a nonlinear quantile map, so adding a smooth level term does not exactly invert it; the add-back is intended for monthly-to-annual means and persistence diagnostics, not for daily quantiles or extremes. Second, the low-frequency signal is itself uncertain: an independent estimate formed the same way from the *raw 20CR* wind differs from the ERA5 one by a median of 0.07 m $s^{-1}$ r.m.s. over the 1940–2015 overlap (Figure 16), reaching 0.30 m $s^{-1}$ in the Po Basin; and before 1979 the ERA5 back-extension carries known low-frequency inhomogeneities, so the pre-1979 add-back is indicative only. The component is provided as a separate, clearly flagged file and is undefined before 1940, where the true slow drift cannot be separated from the network-driven bias.

The seasonal residual correction of Sect. 5, and the four regions calibrated per season, are resolved region by region in Figure 18.

**Uncertainties.** Wherever an uncertainty is quoted on a quantity derived from the daily series, it comes from a block bootstrap. The record is resampled in blocks (whole winters, or thirty-day blocks where winters are not the natural unit) rather than day by day. Consecutive days are not independent, and a naive resample would make every interval far too narrow.

**Drought-duration statistics.** The wind-drought duration and exceedance functions shown in the main text (for example Figure 15) are built from differential event counts per duration bin, not from cumulative distributions, whose neighbouring points share events and carry correlated errors; the counting uncertainties are exact Poisson intervals. Durations are counted only from each region's recommended start (Sect. 6.5), so the network-inflated early-record autocorrelation does not enter the statistics, and confidence intervals on derived quantities come from a whole-winter block bootstrap, which retains the serial dependence a naive resample would miss. Because events are detected within the NDJF window, a drought still under way at a season edge is censored there; re-detecting on a wider October–March window shows that about 3.5 % of events touch a

https://doi.org/10.5194/essd-2026-755
Preprint. Discussion started: 22 October 2026
© Author(s) 2026. CC BY 4.0 License.

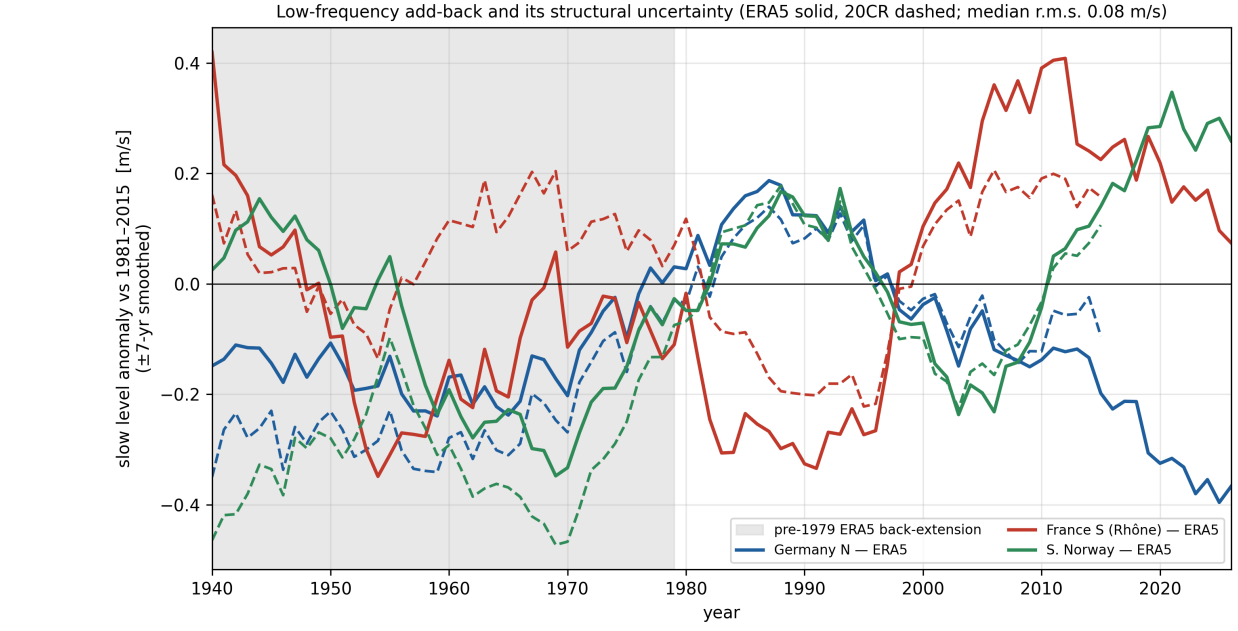



**Figure 16.** The optional low-frequency add-back and its structural uncertainty. Solid line: the ERA5-based slow level anomaly (relative to 1981–2015, ±7-year smoothed) for three regions. Dashed: an independent estimate formed identically from the raw 20CR wind. The two agree to a median of 0.07 m $s^{-1}$ r.m.s. over 1940–2015 across the fourteen regions. The shaded band marks the pre-1979 ERA5 back-extension, where the estimate is less constrained and the two diverge most. The add-back is released as a diagnostic with this uncertainty attached.

boundary and about 1.7 % are genuinely truncated, most in regions where calm spells are least confined to winter. The pooled statistics shift negligibly, though per-region extreme values should be checked for a spell touching a season boundary.

**Independent cross-checks.** The temperature channel is checked against the Central England Temperature series (Parker et al., 1992), daily since 1772 and entirely independent of any reanalysis. The corrected wind is checked against observed wind-power generation and two century-old anemometers (Sect. 7). The full processing scripts and the intermediate data catalogue accompany this manuscript.

https://doi.org/10.5194/essd-2026-755
Preprint. Discussion started: 22 October 2026
© Author(s) 2026. CC BY 4.0 License.

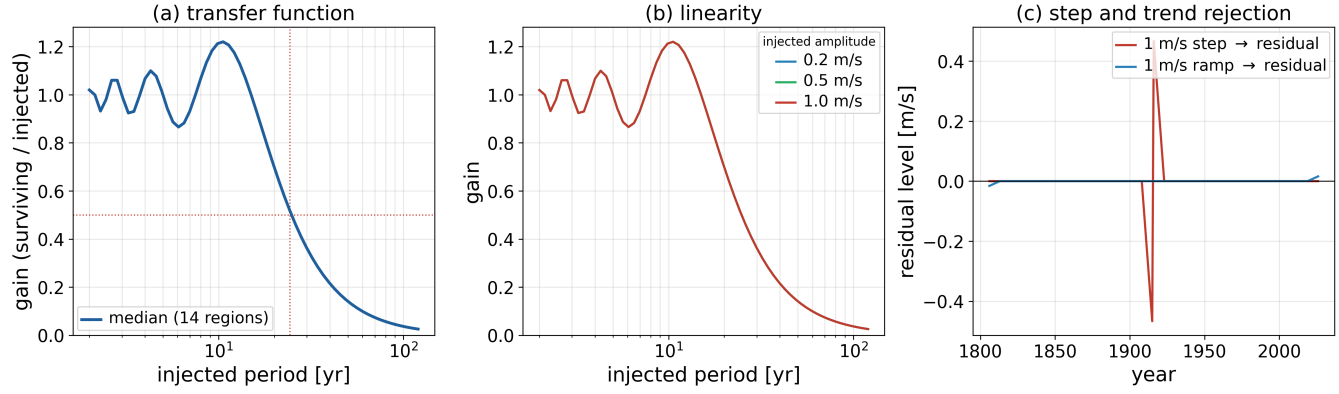



**Figure 17.** Moving-window calibration behaves as an approximately 15-year high-pass filter, verified in three complementary tests. A known level signal is injected into the stationary corrected series and the same calibration is reapplied. **(a)** Transfer function: gain (surviving divided by injected amplitude) remains close to one up to about fifteen years, then declines to half-power near twenty-five years and below 0.1 by sixty. All fourteen regions (grey) collapse onto the median (blue), with an interquartile spread below 0.002, showing that the response is a property of the window rather than the region. **(b)** Linearity: injections of 0.2, 0.5 and 1.0 m $s^{-1}$ give gain curves agreeing within 0.012. **(c)** Step and trend rejection: an injected 1 m $s^{-1}$ step decays to zero residual within about thirty years, while a linear ramp leaves a mean residual of 0.003 m $s^{-1}$. The calibration therefore removes offsets and trends, not only sinusoidal variability. Within ±7 years of either record end the response is degraded by the one-sided window; the two-year point in (a) is an artefact of annual sampling.

## References

Alexandersson, H., Schmith, T., Iden, K., and Tuomenvirta, H.: Trends of storms in NW Europe derived from an updated pressure data set, Climate Research, 14, 71–73, https://doi.org/10.3354/cr014071, 2000.

Azorin-Molina, C. et al.: Homogenization and trends of near-surface wind speed in Spain and Portugal, Journal of Climate, 27, 3692–3712, https://doi.org/10.1175/JCLI-D-13-00652.1, 2014.

Bett, P. E., Thornton, H. E., and Clark, R. T.: European wind variability over 140 yr, Advances in Science and Research, 10, 51–58, https://doi.org/10.5194/asr-10-51-2013, 2013.

Bett, P. E., Thornton, H. E., and Clark, R. T.: Using the Twentieth Century Reanalysis to assess climate variability for the European wind industry, Theoretical and Applied Climatology, 127, 61–80, https://doi.org/10.1007/s00704-015-1591-y, 2015.

Bloomfield, H. C., Brayshaw, D. J., and Charlton-Perez, A. J.: Characterizing the winter meteorological drivers of the European electricity system using targeted circulation types, Meteorological Applications, 27, e1858, https://doi.org/10.1002/met.1858, 2019.

Bundesnetzagentur: SMARD — Strommarktdaten: realised generation, wind onshore and offshore, Germany, 15-minute resolution, 2015–2026, https://www.smard.de, 2026.

Compo, G. P. et al.: The Twentieth Century Reanalysis Project, Quarterly Journal of the Royal Meteorological Society, 137, 1–28, https://doi.org/10.1002/qj.776, 2011.

Cram, T. A. et al.: The International Surface Pressure Databank version 2, Geoscience Data Journal, 2, 31–46, https://doi.org/10.1002/gdj3.25, 2015.

https://doi.org/10.5194/essd-2026-755
Preprint. Discussion started: 22 October 2026
© Author(s) 2026. CC BY 4.0 License.

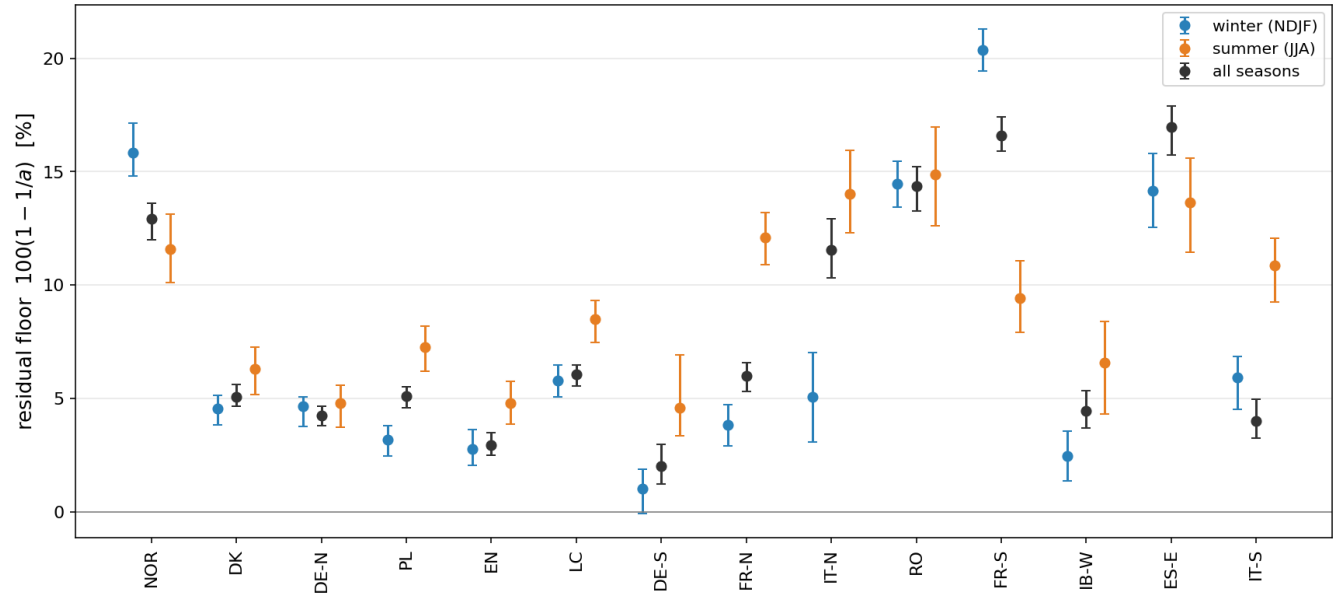



**Figure 18.** The residual correction measured separately by season over the 1940–1980 overlap, for all fourteen regions, on a matched eight-point basis. Winter (NDJF, blue), summer (JJA, orange) and all-season (black) corrections with 95 % winter-block-bootstrap intervals. In the four channelled-seasonal regions (the Rhône corridor, the Po basin, northern France, and southern Norway) the winter correction is distinct from the pooled one, and those regions are calibrated season by season; the other ten keep a single all-season map.

Deutscher Wetterdienst: Climate Data Center, daily climate observations, station 3987 Potsdam (secular station, Telegrafenberg), wind speed, https://opendata.dwd.de/climate_environment/CDC/, 2026.

Feser, F. et al.: Storminess over the North Atlantic and northwestern Europe — a review, Quarterly Journal of the Royal Meteorological Society, 141, 350–382, https://doi.org/10.1002/qj.2364, 2015.

Franke, J., Brönnimann, S., Bhend, J., and Brugnara, Y.: A monthly global paleo-reanalysis of the atmosphere from 1600 to 2005 (EKF400), Scientific Data, 4, 170 076, https://doi.org/10.1038/sdata.2017.76, 2017.

Hersbach, H. et al.: The ERA5 global reanalysis, Quarterly Journal of the Royal Meteorological Society, 146, 1999–2049, https://doi.org/10.1002/qj.3803, 2020.

Hurrell, J. W.: Decadal trends in the North Atlantic Oscillation: regional temperatures and precipitation, Science, 269, 676–679, https://doi.org/10.1126/science.269.5224.676, 1995.

Jiménez, P. A. and Dudhia, J.: Surface wind regionalization over complex terrain: evaluation and analysis, Journal of Applied Meteorology and Climatology, 49, 268–287, https://doi.org/10.1175/2009JAMC2175.1, 2010.

Koninklijk Nederlands Meteorologisch Instituut: Daily weather data of the Netherlands, station 260 De Bilt, daily mean wind speed, https://www.knmi.nl/nederland-nu/klimatologie/daggegevens, 2026.

Krueger, O. and von Storch, H.: Evaluation of an air-pressure-based proxy for storm activity, Journal of Climate, 24, 2612–2625, https://doi.org/10.1175/2011JCLI3913.1, 2011.

https://doi.org/10.5194/essd-2026-755
Preprint. Discussion started: 22 October 2026
© Author(s) 2026. CC BY 4.0 License.





Krueger, O., Schenk, F., Feser, F., and Weisse, R.: Inconsistencies between long-term trends in storminess derived from the 20CR reanalysis and observations, Journal of Climate, 26, 868–874, https://doi.org/10.1175/JCLI-D-12-00309.1, 2013.

Laloyaux, P. et al.: CERA-20C: a coupled reanalysis of the twentieth century, Journal of Advances in Modeling Earth Systems, 10, 1172–1195, https://doi.org/10.1029/2018MS001273, 2018.

Parker, D. E., Legg, T. P., and Folland, C. K.: A new daily Central England Temperature series, 1772–1991, International Journal of Climatology, 12, 317–342, https://doi.org/10.1002/joc.3370120402, 1992.

Paul, S.: Processing and analysis code for the European Geostrophic Wind Reconstruction (EGWR), version 1.0, https://doi.org/10.5281/zenodo.22669767, [Software]. MIT licence, 2026a.

Paul, S.: European Geostrophic Wind Reconstruction (EGWR) Version 1.0: a 220-year daily record of large-scale geostrophic wind for fourteen European regions (1806–2026), https://doi.pangaea.de/10.1594/PANGAEA.997348, [dataset]. Persistent identifier 10.1594/PANGAEA.997348, activated on publication of the dataset, 2026b.

Poli, P. et al.: ERA-20C: an atmospheric reanalysis of the twentieth century, Journal of Climate, 29, 4083–4097, https://doi.org/10.1175/JCLI-D-15-0556.1, 2016.

Robock, A. and Mao, J.: Winter warming from large volcanic eruptions, Geophysical Research Letters, 19, 2405–2408, https://doi.org/10.1029/92GL02627, 1992.

Sigl, M. and Toohey, M.: Volcanic stratospheric sulfur injections from 500 BCE to 1900 CE, eVolv2k version 4, https://doi.org/10.1594/PANGAEA.971968, dataset, 2024.

Slivinski, L. C. et al.: Towards a more reliable historical reanalysis: improvements for version 3 of the Twentieth Century Reanalysis system, Quarterly Journal of the Royal Meteorological Society, 145, 2876–2908, https://doi.org/10.1002/qj.3598, 2019.

Staffell, I. and Pfenninger, S.: Using bias-corrected reanalysis to simulate current and future wind power output, Energy, 114, 1224–1239, https://doi.org/10.1016/j.energy.2016.08.068, 2016.

Valler, V. et al.: ModE-RA: a global monthly paleo-reanalysis of the modern era 1421 to 2008, Scientific Data, 11, 36, https://doi.org/10.1038/s41597-023-02733-8, 2024.

Wang, X. L., Feng, Y., Compo, G. P., et al.: Trends and low frequency variability of extra-tropical cyclone activity in the ensemble of twentieth century reanalysis, Climate Dynamics, 40, 2775–2800, https://doi.org/10.1007/s00382-012-1450-9, 2012.

Wohland, J., Omrani, N.-E., Witthaut, D., and Keenlyside, N. S.: Inconsistent wind speed trends in current twentieth century reanalyses, Journal of Geophysical Research: Atmospheres, 124, 1931–1940, https://doi.org/10.1029/2018JD030083, 2019.

Zhang, Z. et al.: Homogenization of surface wind speed over global land from 1973 to 2022, Journal of Geophysical Research: Atmospheres, 130, https://doi.org/10.1029/2024JD042939, 2025.

Zubiate, L., McDermott, F., Sweeney, C., and O'Malley, M.: Spatial variability in winter NAO–wind speed relationships in western Europe linked to concomitant states of the East Atlantic and Scandinavian patterns, Quarterly Journal of the Royal Meteorological Society, 143, 552–562, https://doi.org/10.1002/qj.2943, 2017.